Computational fluid dynamic simulation of multi-phase flow in fractured porous media during water-alternating-gas injection process

Afzali Shokufe, Rezaei Nima, Zendehboudi Sohrab, Chatzis Ioannis

DOI: 10.1016/j.jhydrol.2022.127852

Computational fluid dynamic simulation of multi-phase flow in fractured porous media during water-alternating-gas injection process

Shokufe Afzali[1], Nima Rezaei[1], Sohrab Zendehboudi[1], Ioannis Chatzis[2]

[1]Department of Process Engineering, Memorial University, St. John's, NL, Canada

[2]Department of Chemical Engineering, University of Waterloo, ON, Canada

Abstract

Naturally fractured reservoirs (NFRs) are among major oil and gas producing reservoirs that are commonly targeted for various enhanced oil recovery (EOR) techniques, particularly water-alternating-gas (WAG) injection. Production from NFRs is complicated due to the flow communication between the matrix and fractures in such porous media. The implementation of WAG injection in NFRs features inherent complexities not only related to the three-phase flow, saturation history, and cycle-dependent hysteresis of the individual phases, but also the fracture-matrix communication, fingering, and early breakthrough of the injected phases particularly during gas injection processes. This paper provides the key results on the computational fluid dynamics (CFD) simulation of WAG injection in a fractured system. We evaluate the impacts of hysteresis, fracture characteristics (aperture, orientation, and fracture density in the network), and the three-phase relative permeability of available phases during the WAG injection. The CFD model simulates an immiscible WAG injection and the CFD results are compared to the experimental data in a strong water-wet sand-pack. Similar to the experiments, we simulate Maroon crude as the oil phase, and synthetic brine, and pure CO_2 at 100 ^oC and atmospheric outlet pressure. The CFD results are in excellent agreement with the experimental data. The absolute relative error is less than 12 % for predicting the ultimate oil recovery factors (RFs) in water flooding (WF) and

gas injection (GI) cycles. Including the three-phase hysteresis significantly increases the accuracy of the WAG process simulation while excluding hysteresis underestimates the instantaneous RFs at each cycle (especially GI cycles) and the ultimate RF by 4%. We also analyze the fracture pattern and configuration; adding fractures to the system increases the system effective permeability, leading to more contact between the injecting fluid and trapped oil, and consequently higher oil recovery. Connecting a vertical fracture to the horizontal fracture enhances the recovery through strong connections between vertical and horizontal blocks. An increase in the fracture aperture from 0.5 to 3 mm increases the RF from 50 % to 59%. The fracture inclination angle from 30^{o} to 90^{o} increased the ultimate RF by only 2 %. Including the gravity forces in vertical model orientation results in overall improvement in RF through engaging both matrix and fracture media in all cycles. As the permeability contrast between the matrix and fracture media decreases, the flow communication between the two regions increases which improves the recovery performance of the WAG process. Our simulation results can help to further understand the effect of various parameters and operational conditions on WAG injection performance in fractured reservoirs.

Keywords: WAG injection; CFD modeling; Fractured reservoirs; Hysteresis effects; Three-phase capillary pressure; Three-phase relative permeability

1 Introduction

Naturally fractured reservoirs (NFRs) contain a substantial portion of the world's remaining oil reserves. They feature complicated production, unforeseeable coupling of wells, instant fracture charges, early breakthrough, and low ultimate recovery (Beydoun, 1998; Zendehboudi et al., 2012). The recovery performances and production mechanisms in fractured- and un-fractured (conventional) reservoirs are inherently different. One of the major factors that impacts the oil recovery from a fractured reservoir is the capillary pressure difference between the fracture and matrix blocks (Firoozabadi, 2000). Experimental data on fracture characteristics, water

breakthrough, and/or relative permeability values are scarce and difficult to obtain. Instead, the application of computer modelling and simulations provides an economical tool to study various factors such as viscous, capillary and gravitational forces at various scales of investigation.

Fractured reservoirs feature complex pore structure heterogeneities that include high flow conductivity in fractures and low contributions to flow in the pore matrix (Elfeel et al., 2016; Zendehboudi et al., 2011a &b). This complexity makes the design of EOR techniques difficult due to poor control of fluid injection into the system, resulting in low sweep efficiency and early breakthrough (Elfeel et al., 2016). Early breakthrough is among all possible problems observed in several case studies, indicating very low overall hydrocarbon recovery in fractured reservoirs (Davidson and Snowdon, 1978; Denoyelle et al., 1988; Panda et al., 2009). In addition, the lack of interconnected fracture networks in NFR systems makes the application of any conventional EOR technique less feasible (Dehghan et al., 2012).

One of the well understood and effective secondary oil recovery methods in petroleum reservoirs is waterflooding (WF) for maintaining the reservoir pressure and displacing the oil toward the production wells. In NFRs, the oil displacement from the matrix blocks is a capillary dominated process, which depends on the wettability of the rock (Behbahani and Blunt, 2005; Firoozabadi, 2000; Schmid and Geiger, 2013; Zendehboudi et al., 2011c). In wettability conditions that are not favorable for the WF process (e.g., mixed-wet to oil-wet), the recovery method can be switched to gas injection (GI), to achieve a higher oil RF. However, the high risk of by-passing oil due to gas high mobility can lead to early gas breakthrough (Panda et al., 2009). In the presence of gravity, the gas breakthrough is delayed upon gas injection to some extent. For such systems, the gas-oil gravity drainage mechanism increases the oil recovery rate in NFRs by providing a driving mechanism as a result of flow communication between the matrix and fracture (Hagoort, 1980; O'Neill, 1988; Van Dijkum and Walker, 1991). Availability of the gas phase in some cases is another limiting factor in the sole deployment of gas injection (as an EOR scenario) into a given NFR.

Numerous EOR field scale projects in fractured carbonate reservoirs are reported since early 1970. Among the reported processes, GI is the most common applied technique with low oil recovery and production rate (Manrique et al., 2007). Also, WF alone is not a successful and common technique in such reservoirs due to very low recovery as a result of by-passing the oil saturated

matrix blocks in the case of an oil-wet reservoir (Shedid, 2006), The three-phase immiscible WAG injection in non-fractured reservoirs has previously been comprehensively studied (Afzali et al., 2019; Afzali et al., 2018; Dong et al., 2005; Van Dijke and Sorbie, 2003); however, the effects of interactions between the matrix and fractures (in fractured media) as well as heterogeneities is overlooked in WAG injection in heterogeneous porous systems.

In one study, it was assumed that WAG injection is not beneficial to be implemented in NFRs (Haghighat, 2004). However, there are successful examples of the application of the WAG injection in fractured reservoirs (Afzali et al., 2018; Awan et al., 2008; Brodie et al., 2012; Christensen et al., 1998). Reservoir heterogeneity directly affects the WAG process efficiency. Many failed EOR projects (in general) are attributed to the reservoir heterogeneity or to the lack of understanding of the petrophysical properties and geology of reservoirs (Donaldson et al., 1989). In highly fractured or stratified reservoirs, the operation of GI is not economical due to high recycle rates and an early breakthrough of the injected gas (Pariani et al., 1992). Because of higher storage capacity of the matrix to trap the crude oil, capillary and gravity forces can significantly impact the recovery from fractured reservoirs, compared to the conventional reservoirs (Gang and Kelkar, 2006; Gilman and Kazemi, 1988). In some NFRs, during a WAG process, water and gas displace each other and by-pass the trapped oil in the matrix pores. Thus, the use of appropriate relative permeability and capillary pressure correlations significantly affects the predictions of flow between the matrix and facture in a porous medium (Elfeel et al., 2016). At the field scale, dual porosity or dual permeability models are commonly applied to calculate the fluid transfer between the matrix and fracture media. Although both models use transfer functions to simplify the exchange rate between two media (namely matrix and fractures), this simplification results in neglecting the heterogeneity that might exist in the matrix, especially in carbonate reservoirs (Al-Kobaisi et al., 2009; Ramirez et al., 2007). Although the WAG injection in fractured reservoirs is difficult to be implemented and not economical, there are a few studies on WAG mathematical modeling and/or simulation in the literature.

Elfeel et al. (2016) analyzed the three-phase flow during WAG injection at two scales (e.g., pore scale and intermediate scale). The latter scale is comparable to a scale of a reservoir; fracture and matrix media are represented using a fine grid model. Their model uses empirical and pore-network modeling systems based on three-phase flow functions to study the effect of gravity and

capillary forces in the matrix-fracture transfer system (Elfeel et al., 2016). Their simulation results highlighted the impacts of the hysteresis in fractured media, which causes up to 10 % difference in predicted oil recovery. However, this difference is smaller in oil-wet systems due to the limited three-phase region, and consequently, less impact is expected from hysteresis (Elfeel et al., 2016). A sensitivity analysis showed that wettability, block geometry, and matrix permeability highly affect the matrix-fracture transfer rates. They also suggested a new multiple interacting continua (MIC) model or a double block model (Elfeel et al., 2016). The proposed model led to more accurate results for fracture-matrix transfer rates at a reduced computational cost (Elfeel et al., 2016).

In another study conducted by Al Eidan et al. (2011), three different injection modes including simultaneous water and gas injection (SWAG), WAG, and continuous gas injection (CGI) were applied in fractured and un-fractured carbonate cores (Al Eidan et al., 2011). They also considered different fracture patterns; at various fracture intensities, they studied the effect of shape factor including elongated slab and sugar cube models. Their simulation results revealed that the improvement in recoveries of SWAG and WAG injection processes over the CGI is related to the higher conformance provided in the water cycles, which controls the CO_2 mobility and decreases its flow through the fracture. It was also reported that the sugar cube model over performs the elongated slab model due to the presence of a vertical fracture in the middle of the core, which helped the gas phase to diffuse into the matrix and to be in contact with more oil (Al Eidan et al., 2011).

Heeremans et al. (2006) performed several fine scale single porosity simulations to extend the flow model to a dual porosity system. The recovery outputs were presented based on two dimensionless numbers of capillary over viscous and gravity over viscous forces. Their generated proxy model optimized the WAG process; it was found that WAG injection increases the final recovery by 10 % higher than WF or CGI (Heeremans et al., 2006). Their model also showed that the shape factor characterizing the nature of the fracture network does not considerably affect the recovery of the system, which was in consistent with field experiences (Heeremans et al., 2006).

Dehghan et al. (2012) performed an experimental study of WAG injection in a micromodel system with fractures. Their micromodel consisted of four matrix blocks surrounded by fractures to examine different scenarios such as continuous WF, CGI (nitrogen as the gas phase), and WAG

injection with various slug injection arrangements. Their results showed that a higher recovery factor (RF) was achieved by WAG injection than continuous WF and CGI in a fractured system. The optimum slug size was reported as 0.08 PV of WF followed by 0.35 PV GI slugs, where the sweep efficiency from matrix blocks was maximized and gas/water production rate was reduced at the outlet. Han (2015) experimentally measured the PVT properties of Bakken crude oil-CO_2. Experiments were performed at six CO_2 concentration levels with three flooding schemes including WF, GI, and miscible CO_2-WAG injection in tight and fractured Bakken formation. They also evaluated the CO_2 soaking effect in the fractured formation. Their results confirmed that breakthrough (BT) occurs much earlier in the fractured formation than the tight system (Han, 2015). Chakravati et al. (2004) conducted a series of core-flood experiments using both homogeneous and fractured cores. They found that WAG injection remarkably delays the BT time (compared to the continuous GI) in the fractured medium and accordingly results in a higher oil recovery.

Agada and Geiger (2014) used a high-resolution simulation model to investigate the effects of non-wetting phase trapping and the miscible and immiscible WAG injection in a heterogeneous (carbonate) reservoir. They showed that the nature of the fracture system has a significant impact on the WAG recovery simulation results, especially in a low-intensity fracture system. However, in a high-intensity fracture reservoir, the fracture system's characteristics become less significant in the recovery process. To obtain the maximum recovery of a WAG process, analyzing and fine-tuning the critical parameters and providing an optimal design of the project are required. Inappropriate designs of WAG parameters in terms of the number of cycles, slug size volume, and injection rates of each WF and GI cycles result in weak process performance, low oil recovery and/or even damaging the formation (Afzali et al., 2018, 2021a&b). Hence, optimization of all affecting factors as well as obtaining a comprehensive knowledge of the reservoir characteristics (e.g., wettability and heterogeneity) helps to more accurately predict and control the gas and water mobility for recovery improvement (Bahagio, 2013; Chen et al., 2010).

Most of the WAG injection studies in the literature are experimental and/or modeling where the porous systems are homogeneous. WAG flooding in heterogeneous/fractured reservoirs is a common process, which is overlooked in available research works. Most of the research investigations conducted on this topic are experimental studies at environment pressure and

temperature, and no mathematical models including reservoir conditions in such cases have been provided so far.

In this study, a robust and reliable computational fluid dynamics (CFD) model using COMSOL Multiphysics® is applied to investigate WAG injection in a fractured system with different fracture configurations, considering three-phase relative permeability and hysteresis. The results of this work provide a comprehensive understanding of fluid flow during WAG injection in a fractured reservoir through a systematic sensitivity analysis on fracture configurations and characteristics, which is useful for designing an optimum WAG injection process in fractured reservoirs.

The paper is structured as follows. After the introduction, the mathematical framework including a description of the CFD model, governing and auxiliary equations, initial and boundary conditions, discretization, and numerical model are provided. We also discuss the limitations in the proposed model. The model is applied to a case study with experimental results to verify our model. After assessing the model with case study data, in the results and discussion section, the effects of various parameters (e.g., fracture patterns and WAG ratio) on the recovery of WAG injection in the fractured system are investigated. Finally, the main conclusions and recommendations for future studies are listed.

2 CFD Modelling of WAG Injection in a Fractured Medium

In this work, we study the three-phase flow during a WAG injection process in porous media with fractures, using COMSOL Multiphysics® software. First, the mathematical framework of the introduced model is described, followed by the numerical formulation, boundary and initial conditions, and numerical simulation.

2.1 Governing Equations

The governing equations for the three-phase flow system (containing gas, oil, and water) include mass balances for all phases, and Darcy's equation for the momentum balance. The gravity effects and dispersion phenomenon are neglected. We study the effect of gravity by changing the alignment of the porous medium. The following equations apply for both the matrix and fracture domains:

$$\frac{\partial}{\partial x}\left[\frac{Kk_{r\alpha}}{\mu_\alpha}\left(\frac{\partial p_\alpha}{\partial x}\right)\right] + \frac{\partial}{\partial y}\left[\frac{Kk_{r\alpha}}{\mu_\alpha}\left(\frac{\partial p_\alpha}{\partial y} + \rho_\alpha . g\right)\right] = \phi \frac{\partial s_\alpha}{\partial t} \qquad \alpha \in \{o, w, g\} \tag{1}$$

where the subscript α denotes the fluid phase which can be oil (o), water (w), and gas (g); p is the pressure; s represents the saturation; g is the gravitational constant; ρ and μ are density and viscosity, respectively; q resembles the source/sink term, which can be the production or injection rate; ϕ and K are the rock porosity and absolute permeability (matrix or fracture), respectively; t is the time; and x introduces the spatial location.

We use the mathematical model to simulate the WAG process in a porous medium including a fracture with higher permeability compare to its surrounding matrix. Therefore, the Darcy's equation is assumed to apply to the fracture, as well.

2.2 Auxiliary Equations

The physical constraint relates the phase saturations of all phases, as given below:

$$\sum_\alpha s_\alpha = s_o + s_w + s_g = 1 \tag{2}$$

where s_o, s_w, and s_g denote the saturations of the oil, water, and gas phases, respectively.

Measurements of the three-phase relative permeability and three-phase capillary pressure in laboratory are highly time-consuming, expensive, and challenging (Virnovsky et al., 2004; Zhou et al., 2016). Hence, it would be of significant importance to use accurate and reliable three-phase relative permeability and three-phase capillary pressure models in the mathematical modeling framework of three-phase flow behavior (such as in WAG). At equilibrium conditions, capillary pressure (p_c) is defined below as the pressure difference between the non-wetting and wetting phases (see Eq. (3)); the capillary pressure is a function of rock properties (ϕ, K, and wettability), fluids saturations, saturation distribution, and the interfacial tension between the phases.

$$p_c = p_{nw} - p_{wet} \tag{3}$$

Here, p_{nw} and p_{wet} are the pressure of the non-wetting and wetting phases, respectively. To avoid confusion with the pressure of water phase (p_w), we use the notation p_{wet} for the pressure of the wetting phase (oil or water). The three-phase capillary pressure model by Neshat and Pope (2017) is used, which is a modified version of Skajaveland et al.'s two-phase capillary pressure model

(Skjaeveland et al., 1998). The proposed capillary pressure model is applicable to all rock wettability condition. Eq.(A1) in Appendix A is used for the three-phase capillary pressure, which is the generalized form of this model—obtained using Gibbs free energy minimization framework (Neshat and Pope, 2017). The entry capillary pressure and capillary exponent values should be estimated from experimental data.

In the two-phase systems (e.g., oil/water, oil/gas, and/or water/gas), there are only two major displacement paths in which the saturation of one phase may decrease or increase. However, in three-phase flow systems, there are infinite numbers of displacement paths (Shahverdi and Sohrabi, 2012). In other words, any three-phase flow system involves variations of the two independent saturations. Hence, measurements of the three phase relative permeability for all possible displacement variations is not practical for the immiscible WAG injection displacement. The WAG process involves an inherent complexity from hysteresis that occurs due to the alternating saturation increase-and-decrease (for wetting and non-wetting phases), corresponding to the imbibition and drainage cycles. Hysteresis is a vital phenomenon that strongly affects the performance of a WAG process (Shahverdi and Sohrabi, 2012). Thus, using a reliable three-phase relative permeability and hysteresis model is an important step in modeling three-phase flow such as in WAG injection process. Larsen and Skauge (1998) developed a relative permeability model based on cyclic hysteresis effects during a WAG injection process. The proposed model is able to capture the reduced mobility and hysteresis loops in three-phase flow. The experimental wetting and non-wetting relative permeability data and the correlation between the maximum non-wetting saturation and trapped non-wetting saturation are limited. Another model was developed by Ranaee et al. (2015) to predict three-phase oil relative permeability based on a sigmoid-based model. Their proposed model considers the key effects of the pore-scale phase distributions within the suggested effective empirical model for oil relative permeability. The sigmoid-based model is capable to generate: (i) the amount of induced remobilization oil by gas injection in a water-wet system; (ii) the transition in layer-drainage regime for low oil saturation ranges; and (iii) the consequent residual oil saturation reduction in a three-phase flow system. Lomeland and Ebeltoft proposed an analytical correlation for three-phase relative permeability and an LET function with an extended version LETx (Ebeltoft, 2013).

In the current work, for the matrix domain, we apply the three-phase relative permeability (including hysteresis effects) proposed by Shahverdi and Sohrabi (2012). Their three-phase relative permeability model coupled with a hysteresis model are used to simulate an immiscible WAG injection process in water-wet systems. The model is verified with the experimental WAG injection data. The proposed model also includes all three sets of two-phase relative permeabilies (i.e. oil-water, oil-gas, and water-gas systems), while most of the proposed models are only valid for two sets of relative permeability systems such as oil-water and oil-gas systems. This model assumes that the three-phase relative permeability ($k_{r\alpha}^{3ph}$) of a given phase α is a function of the two-phase saturations and relative permeabilities for all three phases. The correlations are introduced by Eqs (A2) to (A4) in Appendix A.

For the three-phase relative permeabilities in the fracture domain, we use a model proposed by Lei et al. (2017), as presented by Eqs. (A5) to (A8) in Appendix A. To calculate the capillary pressure in the fracture domain, we use the model suggested Brooks and Corey (1966), which is commonly used in modelling multiphase flow in porous media. The correlation is given by Eqs. (A9) and (A10) in Appendix A.

2.3 Initial and Boundary Conditions

COMSOL Multiphysics® 5.4 uses a graphical user interface (GUI) that enables to model the problem. The analysis of the WAG injection process is performed, using a 2D domain, having two subdomains and eight boundaries for the fractured porous medium studied in this research as shown in Figure 1. The boundary conditions for each boundary is listed in Table 1.

For each phase, the initial conditions s_α (x, z, t=0) are known from the initial phase saturations established in the experiments.

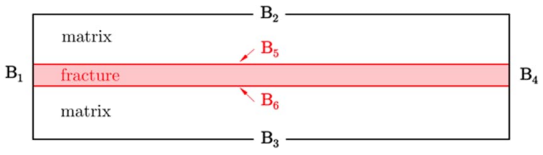

Figure 1: Schematic of fractured model. Boundaries of fractured porous medium during WAG injection for numerical simulation/modeling; the fracture domain is shown with red and matrix is

shown with white. The matrix boundaries are B_1-B_4 and fracture boundaries are B_5 and B_6. The length and width are not scaled for better visibility.

Table 1: Boundary conditions for fractured porous medium in COMSOL Multiphysics®.

Boundary	BC
B_1	q_{inj} = cte
B_2	no flux
B_3	no flux
B_4	$p_o = 0$
B_5	flow continuity
B_6	flow continuity

2.4 Model Discretization and Numerical Method in COMSOL Multiphysics®

The COMSOL Multiphysics® uses a general form of the Darcy's law under the phase transport in porous media module, which is integrated into the continuity equation. The formula is presented for the phase α that can be either the wetting phase (wet), intermediate wetting phase (int-wet) or the non-wetting phases (non-wet), as given below:

$$\delta_{st}.\, C_p \frac{\partial p_\alpha}{\partial t} + \nabla.\left[\delta_k \frac{k_\alpha}{\mu_\alpha}(\nabla p_\alpha + \rho_\alpha \vec{g}\, \nabla h)\right] = \delta_Q Q_\alpha \qquad \alpha \in \{wet, int-wet, non-wet\} \quad (4)$$

where k_α is the effective permeability of phase α. The input parameters are: time scaling factor (δ_{st}), flux scaling factor (δ_k), source scaling factor (δ_Q), storage term (C_p), and source term (Q). The storage term (C_p) is a function of porosity, residual wetting saturation, the effective wetting saturation, and pressure ($Cp = d\theta_w / dh_c$), where θ_w refers to the saturation of the wetting phase, and h_c is the capillary pressure function.

Values of δ_{st} = 0 and 1 are used for the steady state systems and dynamic systems, respectively. δ_k is the flux scaling factor, which is unity in our system; and Q refers to the source term.

For the geometry of the meshes, triangular mesh elements are applied as shown in Figure 2. Later, we compare two different mesh sizes, *coarse* case and *extra-fine* case, to assess the effect of mesh size on the reliability and computational burden of our developed CFD model.

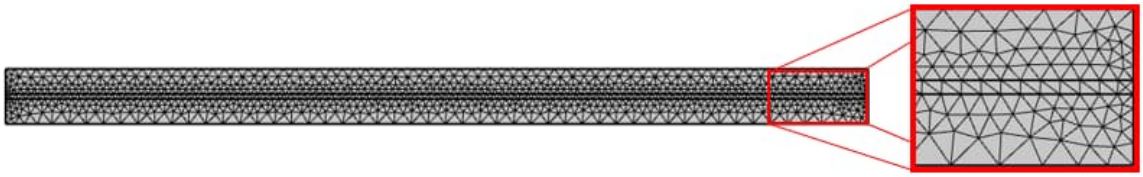

Figure 2: Schematic of model discretization in different regions.

2.5 Model Limitations and Assumptions

In our CFD model, the following assumptions are made:

- 2D fluid flow is considered.
- Except for one case (vertical mode orientation), the effect of the gravity force is neglected.
- The porous medium is incompressible and non-deformable, having a constant porosity.
- The three phases are immiscible, and no reaction occurs between the phases.
- The fluid and rock properties remain constant; no asphaltene precipitation and wettability alteration are considered upon CO_2 injection.
- Hysteresis is neglected in the fracture domain due to its low capillary pressure.
- All WAG injection cycles (both WF and GI) are conducted at a fixed slug size of 0.5 PVI.
- The fracture is modeled as a porous medium with considerably higher permeability and porosity than those in the surrounding matrix. In the experiments, the fracture pore space is created by steel wool (Dorostkar et al., 2009).
- We study an idealized fracture system, containing 3 horizontal and 1 vertical fracture configurations, while a variety of random fracture patterns and configurations are possible in an actual system.

3 Case Study

To verify the simulation results, we use the WAG experimental results reported by Dorostkar et al. (2009). They conducted a series of CO_2-WAG flooding and hot CO_2-WAG flooding in fractured sand packs. In this study, we only use data related to the CO_2-WAG experiments conducted in water-wet and fractured sand packs where the fracture (2 mm aperture) is simulated with a porous medium of higher permeability and porosity. Their experiments were performed at

the atmospheric pressure (to keep the immiscibility condition) and 100°C. Dorostkar et al. (2009) used sand packs with the characteristics summarized in Table 2. They use oil sample from the Maroon oil reservoir in south of Iran. The brine used in their study was synthetic, with a similar composition to the formation brine of the Maroon reservoir. The injected gas was CO_2 with a viscosity and density of 0.0182 cP and 1.6×10^{-3} g/cm^3, respectively (Dorostkar et al., 2009). CO_2 and water were injected into the fractured sand pack at the same rate of 0.5 cm^3/min. The WAG injection tests were continued until no further change in oil production was observed. The properties of the fluids, porous medium, and operating conditions used in the experimental study by Dorostkar et al. (2009) are summarized in Table 2. A schematic of the model is also depicted in Figure 1.

Table 2 : Rock and fluid properties used in this study (taken from Dorostkar et al. (2009)).

Attribute	Variable (unit)	Acting phase(s)	Value
Fluid	ρ (g/cm^3)	g	0.0016
		o	0.8700
		w	0.9970
	μ (cP)	g	0.0182
		o	2.1680
		w	0.2822
	σ (mN/m)	og	50
		ow	75
Porous Medium	K_m (D)		1.1
	K_f (D)		5.0
	ϕ_m		0.28
	ϕ_f		0.85
	L (cm)		35.0
	D (cm)		4.2
	W_f (cm)		0.2
Operating Conditions	s_i (PV)	g	0.000
		o	0.849
		w	0.151
	q (cm^3/min)		0.5
	p (atm)		1
	T (˚C)		100

4 Results and Discussions

In this section, we present the results of the CFD model developed for the WAG injection process and compare it to the experimental data obtained from the case study. We use a relative tolerance

of 1×10^{-4} for the absolute error. The value of the relative tolerance indicates a relative tolerance that controls the accuracy of the geometric representation of the swept object. The geometric representation is an approximation, which is necessary because it is not possible to exactly represent a swept object using NURBS (nonuniform rational basis splines). The default value is 10^{-4} (0.01%); for more details about the relative tolerance, you can refer to COMSOL Multiphysics (2013). A 2D heterogeneous medium with matrix and fracture domains is used, consisting of 2416 domain mesh elements and 1026 boundary mesh elements. Similar to the case study, the fractured sample is initially saturated with oil, and connate water saturation is established prior to starting the WAG injection cycles. Then, it is flooded with alternating injections of water-and-gas cycles. One PV injection (at the flow rate used in the case study) corresponds to 16300 seconds.

We perform parametric sensitivity analysis to study the influence of one factor at a time where other input parameters are held constant. In fact, we do not study the effect of interactions between the input parameters due to high computational time. We consider "One Factor At a Time" (OFAT) so that all factors except one factor are kept constant. Thus, only one parameter varies each time. For instance, to study the fracture aperture on recovery factor, other fracture and matrix characteristics are kept constant as in the reference case; or in the case of changing WAG ratio other operational parameters such as number of cycles and temperature are assumed to be constant.

4.1 Mesh Sensitivity and Analysis

In the COMSOL Multiphysics®, the time-dependent set of equations for fluids flow in porous media are computed using finite element method (FEM). The accuracy of the calculated variables is significantly affected by the mesh properties used in the model. To obtain an optimum mesh configuration and size, we simulate the model using extra fine and coarse triangular meshes for the first waterflooding (WF_1) and first gas injection (GI_1) cycles, and compare the results. To compare the performance of the model using two different mesh sizes, we use measures such as absolute average relative deviation (AARD, in Eq. (5)) and the relative error (see Eq. (6)) in terms of the final recovery factor (RF_{final}) from the experimental data and the CFD model for all of instantaneous *RFs* (N), as expressed below:

$$AARD\ (\%) = \frac{100}{N}\sum_{i=1}^{N}\left(\frac{\left|RF_i^{exp} - RF_i^{sim}\right|}{RF_i^{exp}}\right) \quad (5)$$

$$Error\ (\%) = 100\left|\frac{RF_{final}^{exp} - RF_{final}^{sim}}{RF_{final}^{exp}}\right| \quad (6)$$

The percent error results are given in Table 3 for the RF achieved by the end of the WF_1 and GI_1 cycles. CPU time is also reported in Table 3 , as a measure of computational burden due to mesh size. The time-steps for both cases are fixed and constant.

Table 3: Effect of mesh size on processing time and error percentage for WF_1 and GI_1 cycles.

Mesh	#Nodes	CPU time (s)		% AARD		% Error	
		WF_1	GI_1	WF_1	GI_1	WF_1	GI_1
Extra fine	2416	17	1389	33.6	3.032	0.436	0.96
Coarse	1242	3	1005	34.1	6.241	1.854	9.14

Table 3 reveals that by applying the extra fine mesh (which includes twice as much number of nodes) the CPU time is increased as expected, and the error is decreased (both AARD and relative error). The percentage of relative error in the RF_{final} is more affected by the mesh size for the GI cycle where the error in the ultimate RF is changed by one order of magnitude. For the WF cycle, both extra fine and coarse meshing result in accurate results where the error in the RF_{final} is < 2%. Overall, the GI cycle brings more computational burden, compared to WF. The CPU time for the GI is two orders of magnitude slower than the WF case; this most probably occurs due to the three-phase flow system during GI that involves three-phase relative permeability, hysteresis, and capillary pressure, while in WF1 only two phases (oil and water) exist in the system.

4.2 Model Validation with Experimental Data

The schematic of the WAG injection cycles for the CFD model is illustrated in Figure 3. Each injection mode (WF or GI) volume is 0.5 PV; in the first WAG cycle, WF_1 and GI_1 are conducted; in the second cycle, WF_2 and GI_2 are employed; and finally, in the third cycle, WF_3 is implemented. Because the oil production is insignificant at this stage, the GI_3 stage is abandoned.

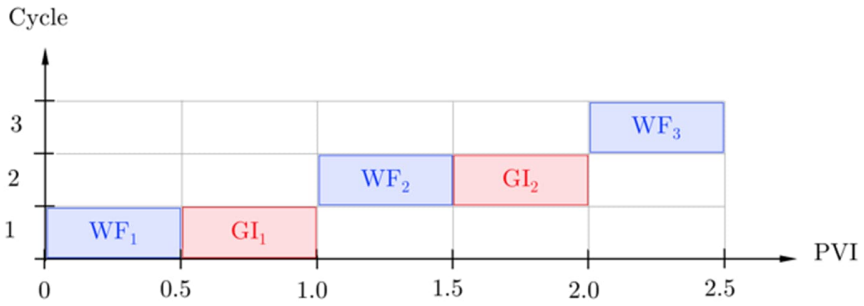

Figure 3: Schematic of WAG cycle injections scheduled in mathematical model.

After developing the CFD model, we compare its performance (outputs) with the experimental data for these 2.5 WAG injection cycles; the comparison is presented in Figure 4. For this simulation, the injection rate is 0.5 cm^3/min, using a WAG ratio of 1.0 and a slug size of 0.5 PV. The WAG ratio is defined as the volume of water slug size in the WF cycles to that of the gas slug in the GI cycles. In this phase, we use constant slug sizes of water and gas in different cycles of water injection (WF_1, WF_2, and WF_3) and gas injection (GI_1 and GI_2), as depicted in Figure 3.

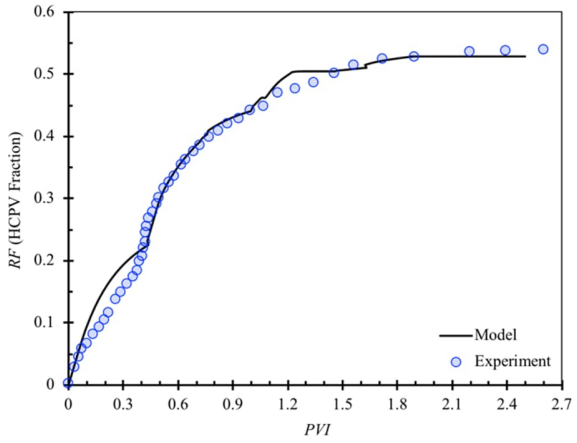

Figure 4: Comparison between the RF of WAG injection in a fractured system from experimental and numerical simulation works (q = 0.5 cm^3/min, slug size = 0.5 PV, and WAG ratio = 1). The solid line shows simulation results and the scatter points are the experimental data from Dorostkar et al. (2009).

The first WAG cycle starts with the injection of water (WF_1) in a two-phase system, with initial oil saturation of s_{oi} =0.849 PV, and initial water saturation of s_{wi} =0.151 PV. In this stage, no gas is present (s_{gi} =0); therefore, two-phase relative permeability and two-phase capillary pressure

models are applied in the WF_1 cycle. As it is clear from Figure 4, after 0.5 PV in WF_1, an oil RF_{final}= 0.23 hydrocarbon pore volume (HCPV) fraction is achieved. Therefore, a large portion of the oil in place is still trapped in the system (s_{or} =0.65 HCPV fraction). The first GI process starts at the initial oil saturation of 0.65 PV and initial water saturation of 0.35 PV, using injection rate q = 0.5 cm^3/min, which is constant during the 0.5 PVI. At this point, due to the presence of gas in the system (in addition to oil and water), three-phase capillary pressure and three-phase relative permeability correlations are utilized. By the end of GI_1 (after 0.5 PVI), a final recovery of 0.45 HCPV fraction is obtained. After the first GI, the second WF, second GI, and finally the third WF are performed in the fractured porous system, after which the RF_{final} =0.53 HCPV fraction and residual final oil saturation of 0.55 are obtained.

Based on Figure 4, the CFD model is capable of capturing the recovery performance behavior as an excellent match is attained between the model results and experimental data of WAG injection in fractured porous medium. A summary of error values when estimating the RF in different WAG cycles is presented in Table 4 , where the relative error is calculated based on RF at the end of each process; the maximum error is achieved during the 0.5 PVI in each process. The proposed CFD model is a suitable tool in estimating the oil RF with a maximum relative error of 12%.

Table 4: Comparison of RF from model and experiments for WAG injection in a fractured porous medium; Experimental data are from Dorostkar et al. (2009).

WAG Attributes		s_{or}	*RF* (HCPV fraction)		Error* (%)	
Cycle	Process	(HCPV fraction)	Exp	Sim	Relative	Max
1	WF_1	0.65	0.220	0.230	-4.50	12.30
	GI_1	0.50	0.448	0.446	0.446	5.60
2	WF_2	0.42	0.502	0.503	-0.126	11.20
	GI_2	0.39	0.528	0.529	-0.189	0.571
3	WF_3	0.38	0.539	0.540	-0.237	0.230

* Relative error is defined based on RF at the end of each process while the maximum error is achieved.

For the simulation results in WF1, two-phase relative permeability and capillary pressure data *a priori* are tuned. To do so, we use the experimental data from the literature and tune the two-phase relative permeability and capillary pressure models employing the pattern search optimization method. This is the reason for the overestimation in WF_1 cycle. We are able to obtain a perfect fit

for this stage; but, prefer not to force the model to match the WAG production data as the recovery at the end of WF_1 is very close to that in the experiments. For the GI_2 to WF_3 cycles, the model parameters are tuned by using the production data of WAG due to unavailability of the three phase capillary pressure and relative permeability behaviors for a system similar to the case study. There is also some overestimation in the RF from our model corresponding to WF_2; however, the ultimate RF is similar to the experimental data. This difference might occur due to the slight change in the wettability of the rock from strongly water-wet to slightly oil-wet during the process.

4.3 Mobility Changes

In this section, we study the effect of mobility of different phases on WAG performance, using the fitted mathematical model. The mobility of each phase and the total mobility of system are calculated using Eqs. (7) and (8):

$$\lambda_\alpha = \frac{K k_{r\alpha}}{\mu_\alpha} \quad \alpha \in \{o, w, g\} \tag{7}$$

$$\lambda_{Tot} = \sum_\alpha \lambda_\alpha \tag{8}$$

where λ_α is the phase mobility; α denotes different phases of oil, water, and gas; $k_{r\alpha}$ and μ_α are the three-phase relative permeability and viscosity of phase α, respectively; and K stands for the absolute permeability.

The interplay between the capillary and viscous forces can be described by the capillary number $N_{Ca}=v\mu/\sigma$ (Chatzis and Morrow, 1984); based on the operating conditions corresponding to the WAG experiments, $N_{Ca} \approx 2\times10^{-7}$ which reveals the dominancy of capillary force compared to viscous force during the WAG flooding process.

Plots of the phase mobility for oil, water, and gas are depicted in Figure 5 for both the matrix and fracture domains and at the middle of the core. The results for gas, water, and oil are consistently shown with red, blue, and black, respectively. Furthermore, the curves of phase mobility in the matrix and fracture are consistently shown with solid, and dashed lines respectively. The symbols of mobility of gas, water, and oil, in the fracture are $G|_f$, $W|_f$, and $O|_f$. Similarly, those for the matrix are distinguished with $G|_m$, $W|_m$, and $O|_m$.

During the primary waterflooding (WF_1), only water (wetting phase) and oil (non-wetting phase) exist in the system. By implementing WF_1 (see Figure 5(a)), the mobility of the water increases, while that of the oil phase decreases. The mobility values of the gas phase in the matrix and fracture are zero because at this stage, there is no gas phase in the system. Water advances into the network of smaller pore spaces in the matrix blocks with a higher imbibition capillary pressure, knowing that water is the wetting phase. For this reason, the mobility of the water in the matrix is much higher than that in the fracture. The oil (non-wetting) phase can flow from the matrix to the fracture with a lower resistance to flow. After WF_1, a high percentage of the oil (s_{or} = 0.65 HCPV fraction) is still trapped in the pores; when gas is injected into the system in GF_1 cycle (in Figure 5(b)), it flows through the fracture, which has a relatively lower entrance capillary pressure, compared to the matrix. Therefore, the mobility of the gas phase in the fracture becomes high. Since the saturation of the oil phase in the fracture is higher than that in the matrix medium, the oil recovery rate (due to increase in the oil mobility in the fracture) increases significantly. Because of the high mobility of the gas phase, total mobility increases in the porous medium in GF_1 cycle. Most of the injected water from WF_1 is trapped in the matrix where the gas phase does not access in GF_1; hence, the mobility of the water in both matrix and fracture media remains constant during GF_1 cycle.

(a) (b)

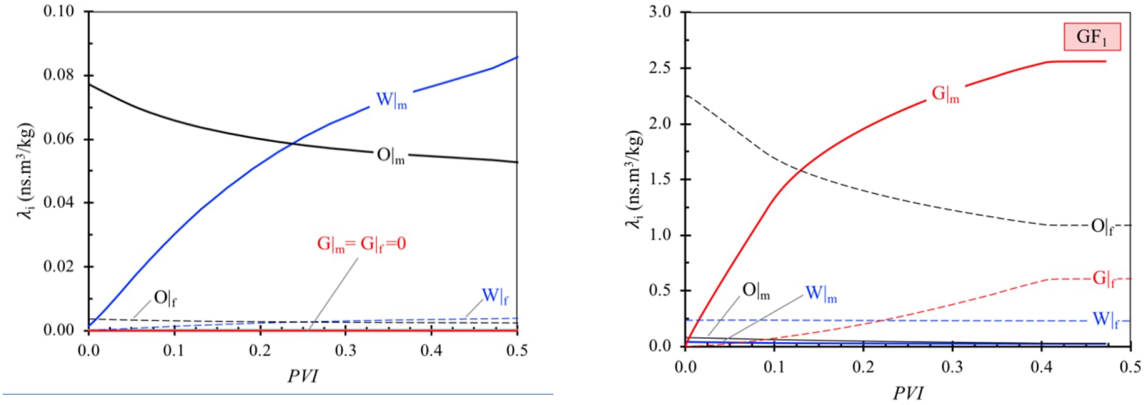

(c) (d)

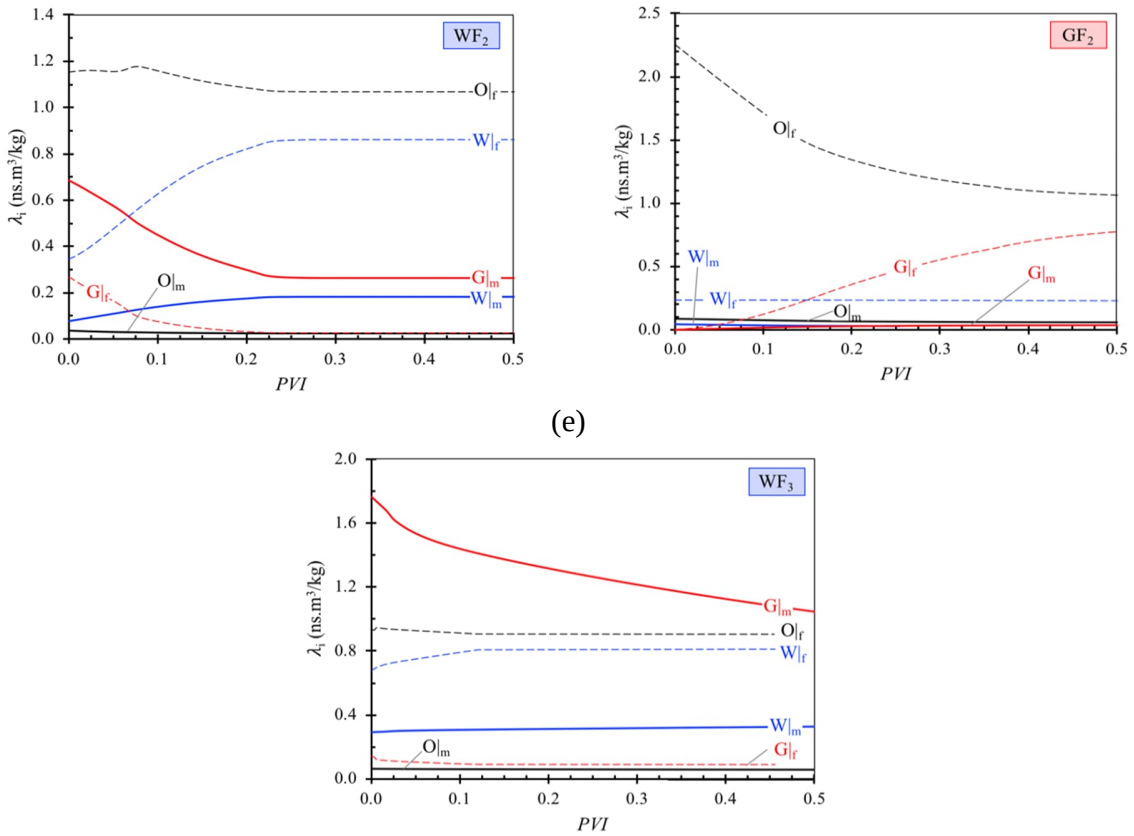

(e)

Figure 5: The phase mobility and total mobility changes of each process in the middle of the core, based on PVI in the matrix zone where (a): primary WF, (b):1st GI, (c): 2nd WF, (d): 2nd GI, and (e):3rd WF.

The mobility profiles for the secondary water injection (WF_2) are illustrated in Figure 5(c). As expected, the mobility of the water phase increases sharply and that of the gas phase decreases. During the second WF (WF2), the dynamics of water mobility in both matrix and fracture is faster than those in the previous water injection cycle (i.e., WF_1). The mobility of the water phase stabilizes sooner (after about 0.2 PVI in Figure 5(c)) in the WF_2 compared to the WF_1. Because water is the most wetting phase, it does not advance through the larger pores (previously invaded by the gas phase). This is especially valid for the water phase in the fracture; consequently, the matrix domain contributes the most to the oil production in WF cycles. For this reason, the mobility of gas phase in the fracture is low, which stabilizes quickly (<0.1 PVI in Figure 5(c)). Because of insignificant production from the matrix zone by the water phase and gas entrapment in the fracture, the mobility of the oil phase does not change appreciably during WF_2. The mobility of different phases during the GI_2 cycle is depicted in Figure 5(d). The mobility of the gas phase increases in both matrix and fracture, while the oil mobility is low, which slightly decreases. This

is due to the oil depletion in the fracture medium upon previous GI cycles. Therefore, there is a percolating pathway for the gas phase (through the fracture) from the injection to the production points which will remain as the preferential pathway for gas. In tertiary waterflooding (WF_3) process, the flow communication between the matrix and fracture is ceased due to the hysteresis effect and high mobility of gas in the fracture as a result of high gas saturation. Therefore, no significant oil production is observed during WF_3. The mobility of the gas phase in the matrix also decreases, and the mobility of the oil and water phases does not significantly change.

4.4 Hysteresis Effect

In this section, we investigate the effect of hysteresis on the performance of WAG, using the tuned model. To model the results without including the hysteresis effects, a different relative permeability model is used that overlooks the hysteresis. Measurements of the three-phase relative permeability are difficult and time-demanding; especially, when the steady-state method is used (Fatemi, 2015). Numerous empirical models such as Stone-I, Stone-II, and Baker are introduced to estimate the three-phase relative permeability values from two-phase data (Baker, 1988; Stone, 1970; Stone, 1973). Various theoretical and experimental studies confirm the dependency of the relative permeability to parameters such as rock and fluid properties including fluid viscosity, interfacial tension, injection rate, wettability, immobile water saturation, pore size distribution, and the saturation history (Avraam and Payatakes, 1999). The dependency of relative permeability to fluid saturation history is described as relative permeability hysteresis, which becomes significant in three-phase flow systems (Fatemi, 2015). Cyclic dependency of the three-phase hysteresis permeability becomes important in tertiary oil recovery processes such as WAG injection and cyclic steam stimulation (CSS) processes (Fatemi, 2015). Simulation studies showed remarkable uncertainties when applying three-phase relative permeability models in gas and WAG injections at field scales (Guzman et al., 1994). The simulation results of oil recovery with and without including hysteresis revealed that a higher oil RF is obtained by incorporating hysteresis effect in relative permeability correlations, compared to the no-hysteresis case (Ghomian et al., 2008). In the case of involving hysteresis effects, a higher oil RF is obtained over a longer period which is attributed to the effect of trapped gas, blocking the oil flow from high-permeability pore spaces.

To study the impact of relative permeability hysteresis on the behavior of three-phase flow in WAG, we use the Stone model (see Eqs. (9)–(13)) (Stone, 1970) which excludes any hysteresis

effects (Stone, 1970). In this phase of the study, we model three cycles of WAG injection with 0.5 PV slug size at WAG injection ratio of 1.0 and operating conditions similar to the previous case with hysteresis.

$$s_o^* = \frac{(s_o - s_{or})}{1 - s_{wc} - s_{or}}, \; s_o \geq s_{or} \tag{9}$$

$$s_w^* = \frac{(s_w - s_{wc})}{1 - s_{wc} - s_{or}} \tag{10}$$

$$s_g^* = \frac{s_g}{1 - s_{wc} - s_{or}} \tag{11}$$

$$B_\alpha = \frac{k_{ro\alpha}}{1 - s_\alpha^*} \tag{12}$$

$$k_{ro}^{3ph} = s_o^* . B_w . B_g \tag{13}$$

where α stands for the phases (oil, water, and gas); B_α is a defined factor; s_{or} and s_{wc} are the residual oil saturation and connate water saturation, respectively; k_{row} introduces the two-phase oil relative permeability for oil-water system; and k_{ro}^{3ph} represents the three-phase oil relative permeability. Similar formulations are applied for the three-phase gas and three-phase water relative permeabilities.

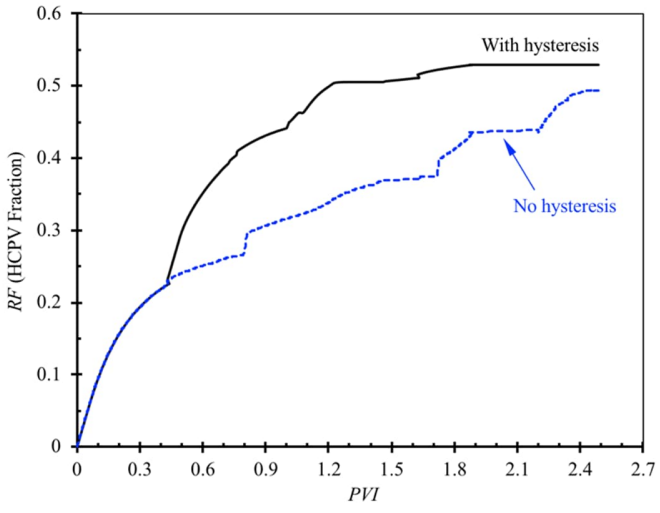

Figure 6: WAG injection RF in two cases of with and without involving the hysteresis three-phase relative permeability effects.

The RF results, using the Stone model are compared with those of WAG injection, considering the hysteresis relative permeability by Shahverdi and Sohrabi (2013) as seen in Eqs. (A2)–(A5)). Figure 6 displays the results of oil recovery with and without the hysteresis effects. As observed in Figure 6, there is no significant difference between the models with and without hysteresis for WF_1 because no gas is present, and water is the most wetting phase. A higher amount of oil is recovered when the three-phase relative permeability hysteresis is considered. This is especially true for the oil recovery in the GI cycles (GI_1 and GI_2). This observation is in agreement with our previous findings that the three-phase relative permeability and capillary pressure affect the non-wetting phase (gas) the most, while they do not considerably affect the behavior of water as the most wetting phase (Afzali et al., 2019). More details on the importance/influence of capillarity and viscous forces during WF_1 are available in the literature (Rezaei and Firoozabadi, 2014). The magnitudes of ultimate oil RF upon injecting 2.5 PV successive cycles of water-and-gas (0.5 PV each) are estimated to be *RF*=0.53 and 0.44 HCPV fraction for the models with and without the three-phase hysteresis, respectively. The higher RF in cyclic injection of water and gas— when the hysteresis effects are considered—may be explained by the gas trapping in the system due to hysteresis that reduces the mobility of the gas phase (see Figure 5(c)). Consequently, this effect will prevent water to flow into the fracture, resulting in a lower water-cut and a lower gas-to-oil ratio. Because the majority of the oil resides in the matrix with smaller pores, the gas trapping in the larger pores (especially in the fracture domain) leads to a higher sweep efficiency. Therefore, a higher oil RF is obtained compared to the case without the three-phase relative permeability hysteresis. This finding is in agreement with micro-scale advancement of phases into small and large pores (Sabti et al., 2016).

4.5 Core Alignment

In the naturally fractured reservoirs (NFRs), pressure-driven mechanisms of producing hydrocarbon may not be an effective strategy for oil production. In such reservoirs, the presence of the fracture, as a highly permeable path, provides a direct channel for the injected fluid (especially the gas phase) towards the production zone, reducing the oil recovery efficiency (Firoozabadi, 1994; Pinder and Gray, 2008). Gravity drainage is reported as an efficient process producing from NFRs (Kazemi, 1990; Kazemi and Gilman, 1993; Sahimi, 2011). Low residual oil

saturation was reported after conducting gravity drainage tests in highly permeable media and in sandstones (Dumore and Schols, 1974).

To examine the effect of gravity forces on the WAG injection performance, a set of immiscible WAG simulation runs are conducted while using the porous media with and without the gravity effects. We change the orientation of the porous medium to account for the gravity by aligning it vertically; due to the small size/width of the porous medium, the gravity effect is minimal in the model that is held horizontally. Figure 7 shows a schematic of horizontal and vertical alignments of the porous system.

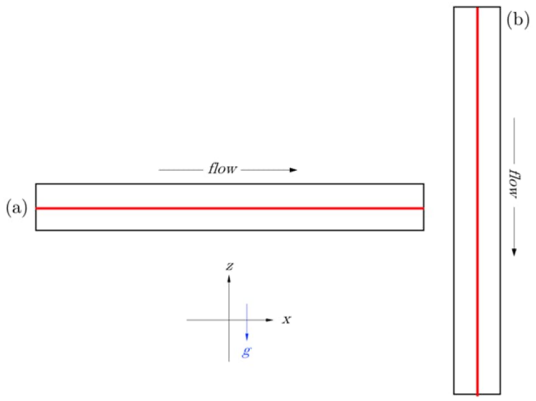

Figure 7: Two different core alignments to investigate the effect of gravity in immiscible WAG injection performance (a): horizontal (along *x*-axis) and (b): vertical (along *z*-axis). The gravity vector *g* is applied in -*z* direction.

For the analysis of gravity impact, all fluid and rock properties and the operational conditions are considered the same for both the horizontal and vertical model alignments. The effect of gravity is demonstrated in Figure 8 from simulation results. The WAG injection scenario is the same as that shown in Figure 3 where the WAG ratio is 1.0, and each WAG cycle is 0.5 PV. According to Figure 8, including the gravity force improves the oil recovery. Due to significant contribution of gravity force in overall driving forces and the flow communication between the matrix and fracture (Zendehboudi et al., 2011a, 2012), the ultimate RF after 2.5 PVI is higher in the vertical mode. The ultimate RF_{final}=0.62 and 0.53 HCPV fraction are achieved in the vertical and horizontal models, respectively, which is about 17% (relative) increase in the RF due to the gravity forces.

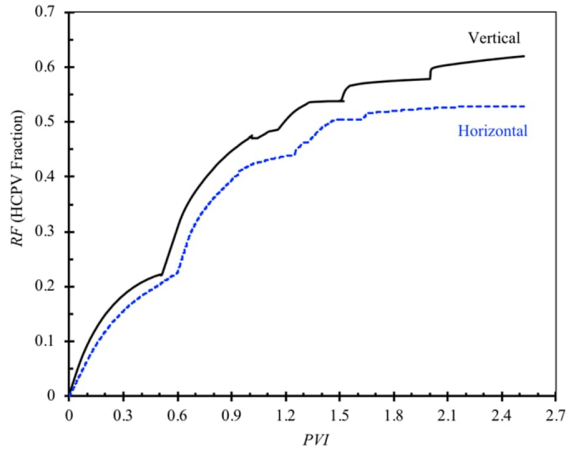

Figure 8: Effect of gravity on *RF* of immiscible WAG injection (WAG ratio = 1 and WAG slug size = 0.5 PV).

In both cases, similar RF values are obtained by the end of WF_1 cycle. However, due to the existence of gravity forces in the vertical case, the instantaneous RFs in the vertical mode are higher. During later cycles, especially during the WF_2 and WF_3 cycles, more oil is recovered in the vertical model, compared to the horizontal case. The presence of gravity also improves the drainage of continuous oil and water films from the pore corners, which is more significant during the later stages of injection cycles when the oil production rate decreases. During the GI cycles, the flow communication can also drive the fluids from the matrix to fracture. This flow communication will postpone the gas breakthrough; as a result, the RF_{final} is higher in the GI cycles when gravity is considered. By sweeping the oil from the matrix to the high permeable fracture medium, the fracture will become the main source for oil production and improve the overall recovery rate from the porous system. The flow of oil from the matrix to fracture is considerably less in the horizontal case without gravity effects. The oil flow from the matrix to fracture postpones the channeling and early breakthrough of the injected fluids especially the gas phase. In WF_3 cycle, the recovery plot reveals that the oil recovery is not ceased in the vertical model even after 0.5 PV. Thus, unlike the recovery behavior in the horizontal model, both matrix and fracture contribute to the oil production when gravity is considered. Further WAG cycles can be injected to increase the ultimate oil recovery in the vertical model.

4.6 Fracture Aperture

The effect of fracture aperture on the oil recovery of the fractured porous system during the WAG injection process is investigated in a set of designed simulation runs (see Table 5). In this section, four porous media with different fracture aperture sizes are simulated to study the oil recovery of WAG injection. All simulated models use the same fluid, fracture, and matrix properties (except for the aperture size). In all cases, a WAG injection scenario similar to that shown in Figure 3 is followed.

Figure 9 illustrates the impact of the fracture aperture on the RF performance during the immiscible WAG injection process. In all cases, a WAG ratio of 1.0, and WAG slug size of 0.5 PV are used. The temperature and pressure are 100˚C and 1 atm, respectively.

Table 5: Effect of fracture aperture on WAG injection.

Fracture aperture (mm)	s_{or} (HCPV fraction)	*RF* (HCPV fraction)
0.5	0.424	0.500
1	0.415	0.511
2	0.399	0.530
3	0.348	0.590

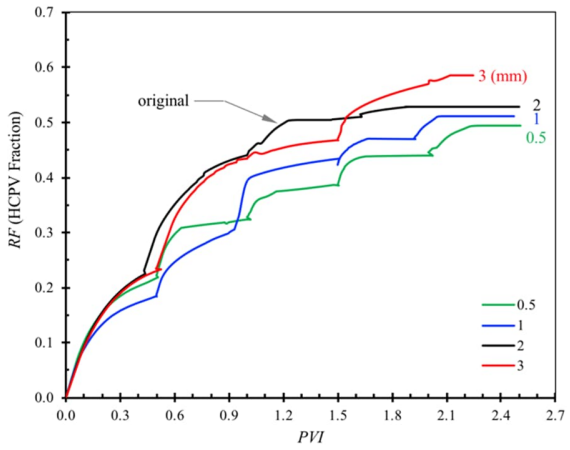

Figure 9: Influence of fracture aperture size on oil recovery performance upon immiscible WAG injection in a fractured medium (q = 0.5 cm^3/min, slug size = 0.5 PV, and WAG ratio = 1).

According to Figure 9 and Table 5, by widening the aperture size of the fracture in the model, the oil recovery of the porous system increases. The model with the 3 mm aperture size results in the highest oil recovery (in each cycle) and reaches the RF_{final} = 0.59 HCPV fraction, at fixed PVI for all cases. Moreover, in the same case, the production is ceased after 2.24 PVI, compared to other cases in which the production is continued for 2.5 PVI. The shorter production time in the cases with higher fracture aperture size is due to the faster drainage of oil from the fracture (that contains more oil) and faster imbibition in the matrix blocks as the water tends to sweep into the matrix blocks rather than the fracture medium. Note that the fracture is simulated in both the model and experiments with a porous domain with a significantly higher porosity and permeability. The fracture has a porosity of about 85%. Because the overall recovery from the fracture is higher than that from the matrix, the overall RF from the fractured model increases with increasing fracture aperture, because the pore volume of oil residing in the fracture increases accordingly. Upon an increase in the fracture aperture, the overall permeability of the model also increases, resulting in a higher recovery rate from the model. At very low aperture values, the fracture block acts similar to the matrix. Looking closely at the instantaneous RFs for the case with the largest fracture aperture size (b=3 mm), most of the jumps in the instantaneous RFs occur during the GI cycles rather than the WF cycles. The ultimate RF obtained during WAG injection in a case with 0.5 mm fracture aperture is 0.5 HCPV fraction.

The discussion on the loss of capillarity in the fracture when the aperture increases above a critical value is not valid in our case study because the fracture medium is a porous medium with higher permeability and porosity for which capillary continuity holds. By increasing the fracture aperture, only the width of this higher permeability region increases, and the critical aperture size will not be materialized. More details about the critical aperture size and its effects on recovery performance is available in the literature (Chatzis et al., 1988; Chatzis and Morrow, 1984; Dejam and Hassanzadeh, 2011; Parsaei and Chatzis, 2011; Zendehboudi et al., 2011b, 2012).

4.7 Permeability Contrast Between Matrix and Fracture

The flow properties of the NFRs are governed by the flow through fracture and matrix and the flow communication between these two regions that is affected by the permeability contrast between the matrix and fracture. To investigate this effective parameter, a set of WAG injection

runs with three different K_m/K_f ratios (by changing the matrix permeability) are conducted. All three cases are conducted with a WAG ratio of 1.0, and constant injection rate of 0.5 cm^3/min, with 2.5 cycles and at the constant PVI of 0.5 for each injection mode (WF or GI). The ratio of K_m/K_f = 0.22 is considered as the base case and two other ratios of K_m/K_f = 0.1 and K_m/K_f = 0.3 are compared with the base case to examine the effect of higher and lower values of this ratio.

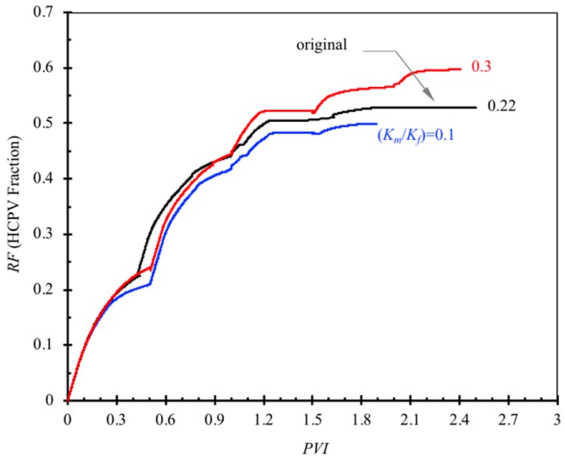

Figure 10: Influence of permeability contrast (K_m/K_f) between matrix and fracture on oil recovery performance upon immiscible WAG injection (q = 0.5 cm^3/min, slug size = 0.5 PV, and WAG ratio = 1).

As the ratio of K_m/K_f increases and approaches unity, the permeability contrast between the matrix block and fracture vanishes. Figure 10 presents the results of permeability contrast comparison according to the RF data versus the PVI. Comparing the simulated results for the case of K_m/K_f = 0.1 and the base case where K_m/K_f = 0.22, it is found that by lowering the matrix permeability the oil recovery significantly decreases—especially during WF injection modes. At K_m/K_f=0.1, and during WF_1 cycle, the water (as the wetting phase) preferrentially invades into the matrix blocks due to high capillary entrance, bypassing the fracture. Because the majority of HCPV resides in the matrix, decreasing the matrix-to-fracture permeability ratio increases the effect of hysteresis, and more oil will be trapped in the matrix. In addition, because the fracture permeability is held constant, by decreasing the matrix-to-fracture permeability, the overall permeability of the porous medium decreases that consequently decreases the rate of oil production. The overall *RF* increases

upon gas injection as the gas phase invades into the fracture medium due to its lower capillary entrance and drains the trapped oil out of that zone. In the second WF, water flows through the lower permeable matrix blocks and has a less chance to sweep the oil towards the producing zone; thus low RF is attained. However, in the second GI, the gas faces a high resistance for entering into the matrix medium and flows through its direct path in the fracture, which is previously drained. Thus, the gas quickly breakthroughs and no significant oil is recovered. The RF_{final} = 0.5 HCPV fraction is obtained in this case (K_m/K_f = 0.1). At a higher matrix-to-fracture permeability ratio of K_m/K_f = 0.3, the WAG injection performance is generally improved in all cycles as demonstrated in Figure 10. A significant increase in the oil recovery is resulted in the WF_1 and WF_2 cycles for the highest permeability contrast ratio, compared to the base case (K_m/K_f = 0.22). At a higher matrix permeability, both the oil recovery and oil recovery rate from the matrix blocks increase upon water injection. Due to less permeability contrast between the matrix and fracture, flow communication between these two regions also enhances and improves the oil recovery from the system. In fact, increasing the matrix permeability increases the chance of the gas phase to invade into the larger pore continuum in the matrix to recover the oil from both the matrix and fracture zones. Therefore, the chance for undesired viscous fingering phenomenon decreases, which causes a delay in the breakthrough (consequently, higher RF at the breakthrough). The ultimate RF_{final} = 0.6 HCPV fraction is obtained after 2.5 cycles of WF and GI in the case of K_m/K_f = 0.3 which is (relatively) 20% higher than the low matrix permeability case of K_m/K_f = 0.1.

4.8 Fracture Inclination

A series of simulation runs are conducted to study the influence of fracture orientation on the RF during the immiscible WAG injection. The simulation runs are performed using a fracture aperture size of 2 mm. We compare the horizontal fracture with three other cases where the fracture is inclined by 30^o, 60^o, and 90^o with respect to the horizontal axis. Figure 11 displays the results of the simulations based on the oil *RF* for 3 cycles of WAG injection with the slug size of 0.5 PVI. According to the results, the ultimate RF values for all cases are so close, between 0.47–0.49 HCPV fraction (Table 2). The ultimate RF is, however, lower than the case of horizontal fracture.

693 **Table 6**: Simulated results of WAG injection in different fractured models.

Inclination (˚)	s_{or} (HCPV fraction)	*RF* (HCPV fraction)
30	0.440	0.471
60	0.442	0.481
90	0.432	0.491

694

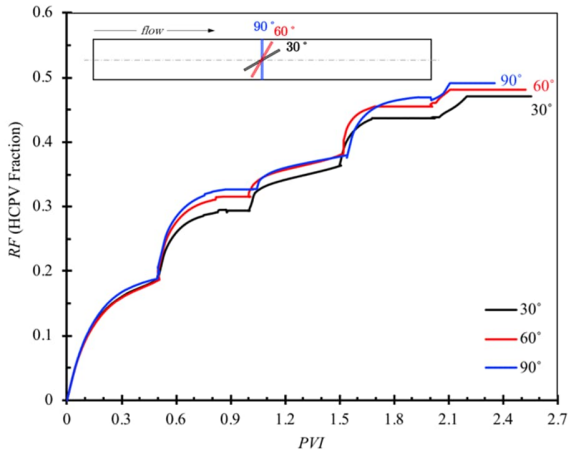

695

696 **Figure 11**: The effect of fracture inclination angle on oil recovery performance upon immiscible
697 WAG injection (q = 0.5 cm^3/min, slug size = 0.5 PV, and WAG ratio = 1).

698

699 During the WF_1 cycle, all three cases have a similar RF performance, which is attributed to the
700 strongly water-wet condition of the system. Since the rock is strongly water-wet, the wetting phase
701 (water) tends to stick to the rock surface as an adhering thin film, and it displaces the oil toward
702 the production zones. During the primary WF, since the system only contains two phases (water
703 and oil), water as the wetting phase prefers to invade into the matrix blocks rather than the fracture.
704 When water reaches the fracture (with any inclination angle) due to low capillary entrance, it
705 bypasses the fracture. Therefore, the fracture inclination angle does not mainly affect the oil
706 recovery during the primary WF. When injecting gas into the system, increasing the inclination
707 angle postpones the gas breakthrough, resulting in a higher RF at the breakthrough condition for
708 the cases with a higher inclination angles. This reveals that the oil drainage from inclined fractures
709 is more facilitated as the gas phase enters the fracture; also, the flow communication between the
710 fracture and matrix blocks is improved. Furthermore, in WF cycles, the difference between

recoveries of different inclination angles becomes less pronounced. This is due to a lower access of water to the fracture medium at any inclination angle. However, in all cycles, the difference in *RF* values of all three cases is not more than 4%.

4.9 Fracture Pattern

Fracture configuration and pattern highly affect the fluid flow in the porous systems. To evaluate the effect of fracture pattern during the WAG injection on oil RF, three different fractured porous media are considered. In Figure 12(a), there is only one fracture in the middle of the horizontal model; the case shown in Figure 12(b) contains two horizontal fractures with similar properties as those in case (a); the model depicted in Figure 12(c) contains one horizontal and one vertical fracture in the middle of the core with the same properties as those for the first two cases. We also compare the performance of cases (a) to (c) with a homogeneous model (without fracture) as illustrated in Figure 12(d).

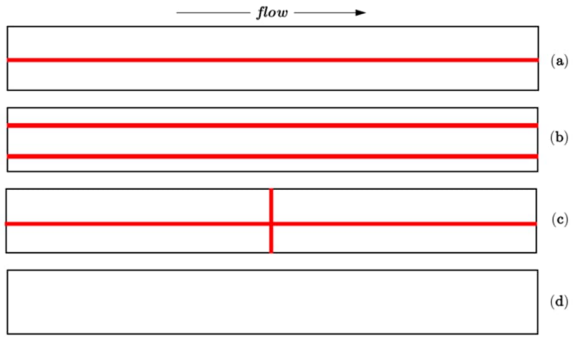

Figure 12: Fracture patterns in different porous media models. Pattern (a) is the original model used in the experiments and pattern (d) is the homogeneous model.

For the WAG injection process in the fracture configurations shown in Figure 12, three cycles of 0.5 PV slugs are injected at a WAG ratio = 1; and the injection flow rate is fixed at 0.5 cm^3/min). Table 7 and Figure 13 report the results of RF for these three cases. According to Figure 13, adding a fracture to the system substantially increases both the instantaneous and ultimate *RFs*.

Table 7: Residual saturation and recovery factors of WAG injection in different models.

Model	s_{or} (HCPV fraction)	*RF* (HCPV fraction)
a	0.380	0.540
b	0.263	0.690
c	0.290	0.658
d	0.250	0.703

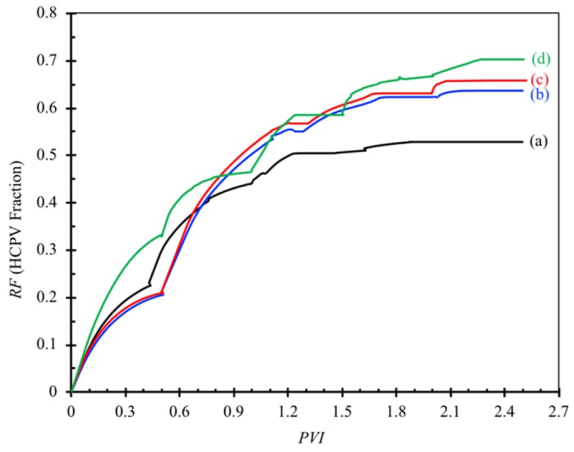

Figure 13: Effect of fracture pattern on the recovery performance of immiscible WAG injection (q = 5 cm^3/min, slug size = 0.5 PV).

As Figure 13 shows, model (d) results in the highest RF with ultimate recovery of 0.71 HCPV fraction after three cycles of WAG injection. The model (c) shows a similar *RF* dynamics compared to the case (b) with ultimate *RF*=0.69 HCPV fraction. Furthermore, model (a) with only one horizontal fracture is the original case that simulates the experimental condition and has the lowest ultimate *RF*=0.54 HCPV fraction among all fractured models. The higher RFs in model (b) and (c) compared to the model (a) occur; because adding fractures to the medium will increase the effective permeability, leading to higher oil production rate and RF. This effect is more pronounced in the first GI cycle, where the gas (non-wetting phase) has a higher chance to invade into the fracture part which the highest oil saturation remained from the previous WF cycle. The injected water (wetting phase) does not advance into the fracture, and it flows to the matrix medium and sweeps the trapped oil in the matrix medium due to the low capillary entrance of the added

fracture. Another reason for a slight increase in the ultimate RF of model (c) over model (b) is related to the inter-connection of the horizontal and vertical fractures where a larger extent of oil communication between matrix and fracture network is possible. This phenomenon occurs if the capillary continuity holds for the vertical fracture in model (c). The capillary continuity will be lost in the vertical fracture if the aperture increases beyond a threshold value, making the capillary pressure insignificant. The importance of the fracture aperture is analyzed in the section 4.6.

Model (b) adds a second horizontal fracture with the same characteristics of the first one (length, and petrophysical properties) while in model (c) the vertical fracture has a less pore volume. This difference is more important when the matrix blocks become the main source for the oil production (especially, during the WF cycles), resulting in more production, and consequently a higher RF from case (c) compared to that in case (b). The highest difference in the RFs of the model (b) and model (c) occurs in the GI_1 process when the gas invades into the fractures, sweeping the oil from the fracture medium; in the GI_2 both models do not contribute appreciably to the oil recovery, and the RFs become comparable between the two models. This is due to the flow of the gas phase into the drained fractures, where the gas directly goes to the producing zone through the fracture (due to less capillary entrance of the fracture and high capillary entrance of matrix blocks). Thus, the gas instantly flows through its preferential path and the condition for breakthrough occurs. After the GI_1 process, most of the recovery from the system is achieved during the WF cycles instead of the GIs, since water phase has a better chance to flow into the matrix blocks (as the main source of oil production) and sweep the trapped oil from that zone. Although the fracture pattern in case (c) shows higher instantaneous RF values compared to case (b), the difference in the ultimate RFs between the two models is less than 2% HCPV.

4.10 Interfacial Tension

One of the main active mechanisms in WAG injection is the interfacial tension reduction. The interfacial tension significantly affects relative permeability curves. For instance, in a completely miscible system, the interfacial tension value is zero and the relative permeability of phases is a linear function of saturation with a slope of 1.0. To study the effect of interfacial tension for oil-water and oil-gas systems on the performance of the WAG injection, the low interfacial tension values ($\sigma_{\text{oil-water}}$=15 mN/m and $\sigma_{\text{oil-gas}}$=10 mN/m) are considered in the simulations (see Figure 14) and the outputs are compared with the results of the original case study.

For both cases, the WAG injection processes are performed at the WAG ratio of 1.0, with 2.5 cycles at 0.5 slug size for each injection mode. According to Figure 14, lowering the interfacial tension in both systems (water-oil and oil-gas) significantly increases the instantaneous and ultimate RF of the WAG process (by 21.76%). The lower interfacial tension facilitates the oil displacement in the matrix zone, where it might be untouched by water, especially during the GI cycles. On the other hand, the amount of trapped gas is strongly affected by the interfacial tension; a lower interfacial tension value results in more gas-oil contact and higher gas entrapment (hysteresis) in the system. Lower interfacial tension also increases the RF of the WF cycles and delays the breakthrough time of the water phase (see Figure 14).

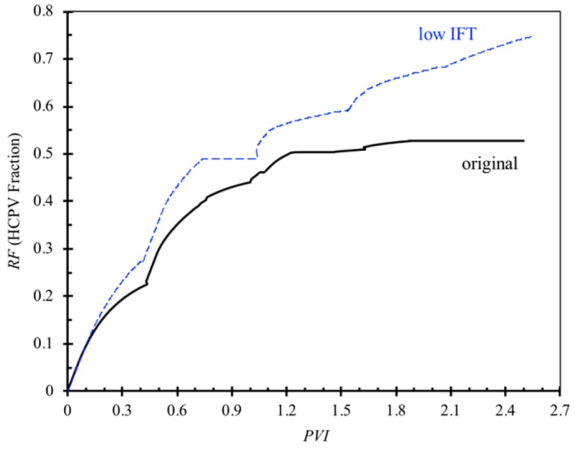

Figure 14: Effect of interfacial tension (IFT) reduction on oil recovery factor during WAG process (q=0.5 cm^3/min, slug size=0.5 PV).

In the last WF cycle (3rd WF), the RF trend reveals that the production is not ceased if the process is continued for further cycles of water and gas injection for the case of low interfacial tension; however, at a higher interfacial tension condition, the RF reaches a plateau in which no more oil is expected to be recovered from the system even by injecting more water and gas.

4.11 WAG Ratio

WAG ratio is 1.0 of the important operating variables in designing a WAG flooding process. Unlike the oil-wet and mixed-wet systems, WAG ratio profoundly affects the fluid flow of the phases during a WAG injection process in a water-wet porous medium (Bunge and Radke, 1982).

To examine the impact of WAG ratio on the performance of WAG process in the fractured porous medium, three different WAG ratios of 1, 0.5, and 0.25 are considered in the model. For the WAG ratios 0.25 and 0.50, the injection rate of the gas is fixed as the original case, and the injection rate of the water is multiplied by 0.25 and 0.5, respectively. Figure 15 describes the simulation results of this sensitivity analysis. According to Figure 15, the highest ultimate RF is obtained at the WAG ratio of 1.0 (*RF* = 52.86%). By decreasing the WAG ratio to 0.5 (*RF* = 47.20 %) and 0.25 (*RF* = 38.74 %), the RF is significantly reduced. WAG injection at a low WAG ratio (e.g., 0.25) results in very low *RF* in the first WF cycle (~6.5 %), compared to two others (11.5% and 22.5% for the WAG ratios of 0.5 and 1, respectively), due to the low injection rate of the water to sweep the entire matrix zone. Because the porous system is strongly water-wet, more RF reduction occurs and the water breakthrough is delayed during the WF cycles, compared to the GI cycles. The rate of oil recovery during the GI cycles exhibits a similar behaviour as the gas (due to the wettability of the system and its preference) mostly flows through the fracture medium.

At higher WAG ratios (e.g., 1), water has a more chance to be in contact with a higher portion of trapped oil bank in small pores and displace more oil. Furthermore, at the WAG ratio of 1.0, two displacing phases of water and gas are traveling at the same velocity in the porous medium, providing a continuous and stable front in which the fluid mobility (especially the gas phase) is controlled; thus, a higher RF is achieved.

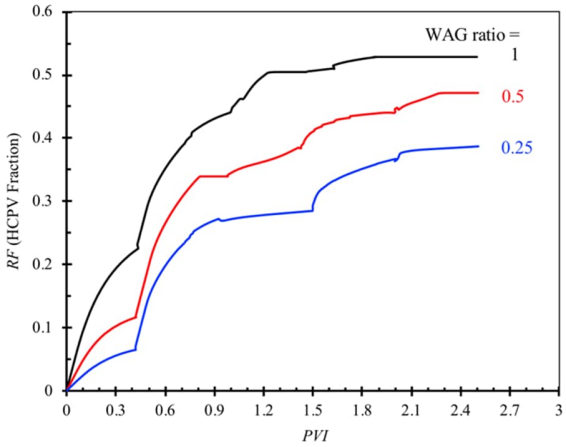

Figure 15: Influence of WAG ratio on recovery factor (2.5 cycles, slug size = 0.5 PV).

The performance of EOR techniques is mostly influenced by the heterogeneity of the targeted reservoirs. WAG injection as a mature EOR technique has been widely used in NFRs. Despite many research and engineering studies conducted on this topic, no comprehensive, robust, and reliable model is provided to simulate immiscible WAG injection in fractured systems. The CFD model proposed in this study uses three-phase relative permeability, hysteresis, and three-phase capillary pressure in a fractured porous medium during immiscible WAG injection. The verified model can be used to study the effect of different parameters including the fracture configuration and pattern, fracture aperture, fracture inclination angle, mobility, and velocities of phases on the recovery performance of WAG injection. This introduced CFD model can be employed by industrial and environmental sectors to avoid additional time and financial costs; it can also help to obtain a comprehensive knowledge of immiscible WAG injection in heterogeneous/fractured reservoirs.

5 Summary and Conclusions

In this study, we simulate immiscible water-alternating-gas (WAG) injection into porous media with fractures, using CO_2 as the gas phase. The mathematical model is implemented in COMSOL Multiphysics® for enhanced oil recovery (EOR) application. The simulations are conducted at atmospheric pressure and at temperature of 100 ^{o}C. Water and gas are sequentially injected at WAG ratio of 1.0, using a slug size of 0.5 PV in a strong water-wet sand pack where Maroon crude is used as the oil phase. In the experimental case study used for model validation, the fracture domain was not an ideal fracture and had been simulated by using steel wool. The following conclusions are obtained from this study:

- The three-phase flow model with three-phase relative permeability and capillary pressure models is reliable in simulating the WAG process in fractured porous media. The maximum error in estimating the recovery factor is 12% when compared to experimental data.
- During the water flooding cycles, the mobility of water and oil in the matrix dominates the overall fluid mobility while in the gas injection cycles, the mobility of the gas and oil in the fracture dominates the overall fluid mobility.

- Including hysteresis in the model results in a higher ultimate oil recovery after 2.5 PVI. With and without hysteresis, the ultimate oil recovery factor values are 0.53 and 0.49 HCPV fraction, respectively.
- The hysteresis effects are mostly due to the gas trapping in the larger pores (such as those in fracture).
- Having a vertical fracture connected to a horizontal fracture in the system enhances the oil recovery by improving the matrix-fracture flow communication.
- Increasing the fracture aperture increases the RF and recovery rate of the oil phase. However, at later cycles, the early gas breakthrough reduces the incremental recovery.
- Fracture inclination angle does not remarkably change the ultimate RF; by changing the inclination angle from 30^o to 90^o, the RF is increased only by 2%.
- Including the gravity forces in the vertical systems causes an overall improvement in RF through engaging both matrix and fracture media in all cycles. It increases the RF by 9%, compared to the horizontal model where no gravity force is active.
- As the permeability contrast between the matrix and fracture parts decreases, the flow communication between the two regions increases and improves the recovery performance of the WAG process.
- Lowering the IFT between phases significantly increases the oil recovery by providing more contact between phases.
- At a WAG ratio of 1.0, the highest oil recovery is obtained, while by lowering the WAG ratio, the fluid front is not stable and less oil is recovered from the system.
- In the current study, we focused on immiscible WAG injection. It is recommended that the miscible WAG injection in heterogeneous reservoirs is examined in future work.

ACKNOWLEDGEMENTS

The authors would like to acknowledge the financial support provided by Memorial University (NL, Canada), Natural Sciences and Engineering Research Council of Canada (NSERC), InnovateNL (formerly RDC), and Equinor (formerly Statoil) Canada.

Appendix A: Governing Equations and Correlations

Three-phase capillary pressure correlation used in this study was proposed by Neshat and Pope (2017), as follows:

$$p_{co\alpha,m} = \sigma_{o\alpha} cos(\theta_{o\alpha}) \sqrt{\frac{\phi}{K}} \times \left[\frac{c_o}{\left(\frac{s_o - s_{or}}{1 - s_{or}}\right)^{a_o}} + \frac{c_\alpha}{\left(\frac{s_\alpha - s_{\alpha r}}{1 - s_{\alpha r}}\right)^{a_\alpha}} \right] \qquad \alpha \in \{w, g\} \tag{A1}$$

where $p_{co\alpha,m}$ is the three-phase capillary pressure between phase oil (o) and phase α (w or g); the subscript m refers to the matrix domain; $\sigma_{o\alpha}$ and $\theta_{o\alpha}$ are the interfacial tension and contact angle between phases o and α, respectively; c_o and c_α are the entry capillary pressure for the phases o and α, respectively; s stands for the phase saturation; and a_o and a_α symbolize the capillary exponent of phase oil and phase α, respectively (Neshat and Pope, 2017).

Three-phase relative permeability model proposed by Shahverdi and Sohrabi (2012) is given below:

$$k_{ro,m}^{3ph}(s_w, s_g) = \frac{\overline{s_o}}{(1-\overline{s_g})(1-\overline{s_w})} [k_{row} k_{rwg} + k_{rog} k_{rgw}] \tag{A2}$$

$$k_{rw,m}^{3ph}(s_o, s_g) = \frac{\overline{s_w}}{(1-\overline{s_g})(1-\overline{s_o})} [k_{rwo} k_{rog} + k_{rwg} k_{rgo}] \tag{A3}$$

$$k_{rg,m}^{3ph}(s_w, s_o) = \frac{\overline{s_g}}{(1-\overline{s_o})(1-\overline{s_w})} [k_{rgo} k_{row} + k_{rgw} k_{rwo}] \tag{A4}$$

where $k_{r\,\alpha\beta,m}$ is the two-phase relative permeability of phase α in the presence of phase β in the matrix; and $\overline{s_\alpha}$ introduces the normalized saturation of phase α that depends on the flow direction (imbibition/drainage) and the initial state of the grid block, as given below (Shahverdi and Sohrabi, 2013):

$$\overline{s_\alpha} = \frac{s_\alpha - s_\alpha^*}{1 - s_w^* - s_o^* - s_g^*} \qquad \alpha \in \{o, w, g\} \tag{A5}$$

In Eq. (A5), the s_α^* values are defined based on different injection fluid scenarios, as listed in Table A1.

894

895

896

897 **Table A1**: Parameters used in the three-phase relative permeability model in matrix medium.

Three-phase relative permeability	Model parameters	WAG injection cycle		
		Gas	Oil	Water
$k_{rg,m}^{3ph}$	s_g^*	s_g^{start}	s_{gt}	s_{gt}
	s_w^*	s_{wc}	s_{wc}	s_w^{start}
	s_o^*	0	s_o^{start}	s_{ot}
$k_{ro,m}^{3ph}$	s_g^*	0	s_{gt}	s_{gt}
	s_w^*	s_{wc}	s_{wc}	s_w^{start}
	s_o^*	s_{org}	s_o^{start}	s_{ot}
$k_{rw,m}^{3ph}$	s_g^*	0	0	0
	s_w^*	s_{wc}	s_{wc}	s_{wc}
	s_o^*	0	0	0

898

899 In Table A1, s_α^{start} is the saturation of phase α at the beginning of phase α injection process; and
900 s_{gt} and s_{ot} denote the trapped/residual saturations of gas and oil, respectively. Eqs. (A1) to (A5)
901 are used for the matrix domain.

902 Three-phase relative permeability correlations in the fracture part are listed below:

$$k_{rw,f}^{3ph} = \frac{{s_w}^3}{2}(3 - s_w) \tag{A6}$$

$$k_{rg,f}^{3ph} = {s_g}^2\left({s_g}^2 + \frac{\mu_g}{\mu_w}\left(3s_w - \frac{3}{2}{s_w}^2\right) + \frac{\mu_g}{\mu_o}\left(3s_g s_o + \frac{3}{2}{s_o}^2\right)\right) \tag{A7}$$

$$k_{ro,f}^{3ph} = {s_o}^2\left({s_o}^2 + \frac{\mu_o}{\mu_w}\left(3s_w - \frac{3}{2}{s_w}^2\right) + \frac{3}{2}s_g s_o\right) \tag{A8}$$

903 where $k_{r\alpha,f}^{3ph}$ is the three-phase relative permeability of phase α (i.e. oil, water, and gas) in the
904 fracture domain; s_α refers to the saturation of phase α; and μ_α resembles the viscosity of phase α
905 in the fracture.

906 According to the Brooks and Corey model, the capillary pressure of the phase oil-α is expressed
907 below:

$$p_{co\alpha,f} = p_{d\alpha}(s_{e\alpha})^{-\frac{1}{\lambda}} \qquad \alpha \in \{w, g\} \tag{A9}$$

$$s_{e\alpha} = \frac{s_\alpha - s_{r\alpha}}{1 - s_{r\alpha}} \qquad \alpha \in \{w, g\} \tag{A10}$$

where $p_{d\alpha}$ denotes the entry capillary pressure of phase α, which is the minimum pressure for the non-wetting phase to displace the wetting phase from the largest pore accessible. The parameter λ is a measure of pore size distribution and describes the uniformity of the sand particles; and $s_{r\alpha}$ represents the residual saturation of the wetting phase α.

Two-phase relative permeability correlations proposed by Hirasaki (1975) are given below:

$$k_{rw} = k_{rw}^0 S_D^{n_w} \tag{A11}$$

$$k_{rnw} = k_{rnw}^0 (1 - S_D)^{n_{nw}} \tag{A12}$$

$$S_D = \frac{s_w - s_{wi}}{1 - s_{wi} - s_{nwr}} \tag{A13}$$

where k_{rw} and k_{rnw} are the two-phase relative permeabilities of the wetting phase and non-wetting phase, respectively. The k_{rw}^0 and k_{rnw}^0 introduce the end point relative permeability values of the wetting and non-wetting phases, respectively. The n_w, and n_{nw} introduce the wetting phase and non-wetting phase exponents, respectively. The endpoint relative permeability and relative permeability exponents of both wetting phase and non-wetting phase for all three systems (i.e. oil-water, water-gas, and oil-gas) are tuned using the experimental data from the literature where the pattern search optimization technique is employed.

NOMENCLATURES

Acronyms

AARD	Average absolute relative deviation

925	CFD	Computational fluid dynamics
926	EOR	Enhanced oil recovery
927	FAWAG	Foam assistant water alternating gas injection
928	FEM	Finite element method
929	GI	Gas injection
930	HCPV	Hydrocarbon pore volume
931	IOR	Improved oil recovery
932	IWAG	Immiscible WAG
933	M	Mobility ratio
934	NFR	Natural fractured reservoir
935	PVI	Pore volume injection
936	PVT	Pressure volume temperature
937	RF	Recovery factor
938	SWAG	Simultaneous water and gas injection
939	WF	Waterflooding
940	WAG	Water-alternating-gas injection

941

942 **Variables and Parameters**

943	a	Capillary exponent
944	B	Three-phase relative permeability factor (Stone model)
945	c	Capillary entry pressure
946	C_p	Storage term
947	D	Diameter

g	Gravity acceleration constant
h	Height
L	Length
K	Absolute permeability
k_α	Effective permeability of the phase α
k_{rij}	Relative permeability of phase i in the ij two-phase system
k_{ri}^{3ph}	Three-phase relative permeability of phase i
N_{ca}	Capillary number
p	Pressure
p_{di}	Fracture entry pressure of phase i
Q	Source term
s	Phase saturation
t	Time
T	Temperature
v	Velocity
W	Width
x	x-axis coordinate (horizontal)
z	z-axis coordinate (vertical)

Greek Letters

α	Phase (gas, oil, and water)
δ	Scaling factor
ϕ	Porosity

λ	Mobility; Pore size distribution index
μ	Viscosity
ρ	Density
θ	Contact angle
σ	Interfacial tension

Subscripts and Superscripts

c	Capillary pressure
f	Fracture
final	Final state
g	Gas phase
k	Flux (in scaling factor)
m	Matrix
o	Oil phase
og	Oil-gas system
Q	Storage (in scaling factor)
ow	Oil-water system
w	Water phase
wg	Water-gas system
r	Residual phase
st	Time (in scaling factor)
Tot	Total

References

Afzali, S., Ghamartale, A., Rezaei, N., Zendehboudi, S., 2019. Mathematical modeling and simulation of water-alternating-gas (WAG) process by incorporating capillary pressure and hysteresis effects. Fuel: 116362.

Afzali, S., Rezaei, N., Zendehboudi, S., 2018. A comprehensive review on enhanced oil recovery by water alternating gas (WAG) injection. Fuel, 227: 218-246.

Afzali, S., Zendehboudi, S., Mohammadzadeh, O., Rezaei, N., 2021a, Hybrid mathematical modelling of three-phase flow in porous media: Application to water-alternating-gas injection. Journal of Natural Gas Science and Engineering, 94: 103966.

Afzali, S., Mohamadi-Baghmolaei, M., Zendehboudi, S., 2021b. Application of Gene Expression Programming (GEP) in Modeling Hydrocarbon Recovery in WAG Injection Process. Energies, 14 (21): 7131.

Agada, S., Geiger, S., 2014. Wettability, trapping and fracture-matrix interaction during WAG injection in fractured carbonate reservoirs, SPE Improved Oil Recovery Symposium. Society of Petroleum Engineers.

Al-Kobaisi, M., Kazemi, H., Ramirez, B., Ozkan, E., Atan, S., 2009. A critical review for proper use of water/oil/gas transfer functions in dual-porosity naturally fractured reservoirs: part II. SPE Reservoir Evaluation & Engineering, 12(02): 211-217.

Al Eidan, A.A., Mamora, D.D., Schechter, D.S., 2011. Experimental and Numerical Simulation Studies of Different Modes of CO2 Injection in Fractured Carbonate Cores, SPE Enhanced Oil Recovery Conference. Society of Petroleum Engineers.

Avraam, D., Payatakes, A., 1999. Flow mechanisms, relative permeabilities, and coupling effects in steady-state two-phase flow through porous media. The case of strong wettability. Industrial & engineering chemistry research, 38(3): 778-786.

Awan, A.R., Teigland, R., Kleppe, J., 2008. A survey of North Sea enhanced-oil-recovery projects initiated during the years 1975 to 2005. SPE Reservoir Evaluation & Engineering, 11(03): 497-512.

Bahagio, D., 2013. Ensemble Optimization of CO2 WAG EOR.

Baker, L., 1988. Three-phase relative permeability correlations, SPE Enhanced Oil Recovery Symposium. Society of Petroleum Engineers.

Behbahani, H., Blunt, M.J., 2005. Analysis of imbibition in mixed-wet rocks using pore-scale modeling. Spe Journal, 10(04): 466-474.

Beydoun, Z.R., 1998. Arabian plate oil and gas: why so rich and so prolific? Episodes-Newsmagazine of the International Union of Geological Sciences, 21(2): 74-81.

Brodie, J.A., Jhaveri, B.S., Moulds, T.P., Mellemstrand Hetland, S., 2012. Review of gas injection projects in BP, SPE Improved Oil Recovery Symposium. Society of Petroleum Engineers.

Brooks, R.H., Corey, A.T., 1966. Properties of porous media affecting fluid flow. Journal of the irrigation and drainage division, 92(2): 61-90.

Bunge, A., Radke, C., 1982. CO2 flooding strategy in a communicating layered reservoir. Journal of Petroleum Technology, 34(12): 2,746-2,756.

Chatzis, I., Kantzas, A., Dullien, F., 1988. On the investigation of gravity-assisted inert gas injection using micromodels, long Berea sandstone cores, and computer-assisted tomography, SPE Annual Technical Conference and Exhibition. Society of Petroleum Engineers.

1038 Chatzis, I., Morrow, N.R., 1984. Correlation of capillary number relationships for sandstone. Society of
1039 Petroleum Engineers Journal, 24(05): 555-562.
1040 Chen, S., Li, H., Yang, D., Tontiwachwuthikul, P., 2010. Optimal parametric design for water-alternating-
1041 gas (WAG) process in a CO2-miscible flooding reservoir. Journal of Canadian Petroleum
1042 Technology, 49(10): 75-82.
1043 Christensen, J.R., Stenby, E.H., Skauge, A., 1998. Review of WAG field experience, International petroleum
1044 conference and exhibition of Mexico. Society of Petroleum Engineers.
1045 Davidson, D., Snowdon, D., 1978. Beaver River Middle Devonian Carbonate: Performance review of a high-
1046 relief, fractured gas reservoir with water influx. Journal of Petroleum Technology, 30(12): 1,672-
1047 1,678.
1048 Dehghan, A., Ghorbanizadeh, S., Ayatollahi, S., 2012. Investigating the fracture network effects on sweep
1049 efficiency during WAG injection process. Transport in porous media, 93(3): 577-595.
1050 Dejam, M., Hassanzadeh, H., 2011. Formation of liquid bridges between porous matrix blocks. AIChE
1051 journal, 57(2): 286-298.
1052 Denoyelle, L., Bardon, C., Couve de Murville, E., 1988. Interpretation of a CO2/N2 injection field test in a
1053 moderately fractured carbonate reservoir. SPE Reservoir Engineering, 3(01): 220-226.
1054 Donaldson, E.C., Chilingarian, G.V., Yen, T.F., 1989. Enhanced oil recovery, II: Processes and operations.
1055 Elsevier.
1056 Dong, M., Foraie, J., Huang, S., Chatzis, I., 2005. Analysis of immiscible water-alternating-gas (WAG)
1057 injection using micromodel tests. Journal of Canadian Petroleum Technology, 44(02).
1058 Dorostkar, M., Mohebbi, A., Sarrafi, A., Soltani, A., 2009. A laboratory study of hot WAG injection into
1059 fractured and conventional sand packs. Petroleum Science, 6(4): 400-404.
1060 Dumore, J., Schols, R., 1974. Drainage capillary-pressure functions and the influence of connate water.
1061 Society of Petroleum Engineers Journal, 14(05): 437-444.
1062 Ebeltoft, F.L.E., 2013. Versatile Three-Phase Correlations for Relative Permeability and Capillary Pressure,
1063 International Symposium of the Society of Core Analysis, Napa Valley, California, USA. SCA, pp. 1-
1064 14.
1065 Elfeel, M.A., Al-Dhahli, A., Geiger, S., van Dijke, M.I., 2016. Fracture-matrix interactions during immiscible
1066 three-phase flow. Journal of Petroleum Science and Engineering, 143: 171-186.
1067 Fatemi, S.M., 2015. Multiphase flow and hysteresis phenomena in oil recovery by water alternating gas
1068 (WAG) injection, Heriot-Watt University.
1069 Firoozabadi, A., 1994. Research program on fractured petroleum reservoirs. Quarterly report, January 1--
1070 March 31, 1994, Reservoir Engineering Research Inst., Palo Alto, CA (United States).
1071 Firoozabadi, A., 2000. Recovery mechanisms in fractured reservoirs and field performance. Journal of
1072 Canadian Petroleum Technology, 39(11).
1073 Gang, T., Kelkar, M.G., 2006. History matching for determination of fracture permeability and capillary
1074 pressure, SPE Annual Technical Conference and Exhibition. Society of Petroleum Engineers.
1075 Ghomian, Y., Pope, G.A., Sepehrnoori, K., 2008. Hysteresis and field-scale optimization of WAG injection
1076 for coupled CO2-EOR and sequestration, SPE Symposium on Improved Oil Recovery. Society of
1077 Petroleum Engineers.
1078 Gilman, J.R., Kazemi, H., 1988. Improved calculations for viscous and gravity displacement in matrix blocks
1079 in dual-porosity simulators (includes associated papers 17851, 17921, 18017, 18018, 18939,
1080 19038, 19361 and 20174). Journal of petroleum technology, 40(01): 60-70.
1081 Guzman, R., Domenico, G., Fayers, F., Aziz, K., Godi, A., 1994. Three-phase flow in field-scale simulations
1082 of gas and wag injections, European Petroleum Conference. Society of Petroleum Engineers.
1083 Haghighat, S., 2004. WAG Modeling in Fractured Reservoirs, Thesis Report MTA/PW/04-15 TU Delft.
1084 Hagoort, J., 1980. Oil recovery by gravity drainage. Society of Petroleum Engineers Journal, 20(03): 139-
1085 150.

Han, L., 2015. Optimum Water-Alternating-Gas (CO2-WAG) Injection in the Bakken Formation, Faculty of Graduate Studies and Research, University of Regina.

Heeremans, J.C., Esmaiel, T.E., Van Kruijsdijk, C.P., 2006. Feasibility study of WAG injection in naturally fractured reservoirs, SPE/DOE symposium on improved oil recovery. Society of Petroleum Engineers.

Hirasaki, G.J., 1975. Sensitivity coefficients for history matching oil displacement processes. Society of Petroleum Engineers Journal, 15(01): 39-49.

Kazemi, H., 1990. Naturally fractured reservoirs, Third International Forum on Reservoir Simulation, Baden, Austria.

Kazemi, H., Gilman, J., 1993. Multiphase flow in fractured petroleum reservoirs, Flow and Contaminant Transport in Fractured Rock. Elsevier, pp. 267-323.

Larsen, J., Skauge, A., 1998. Methodology for numerical simulation with cycle-dependent relative permeabilities. SPE Journal, 3(02): 163-173.

Lei, G., Wang, C., Yuan, T., Yang, L., 2017. An Analytical Equation to Predict Oil-Gas-Water Three-Phase Relative Permeability Curves in Fractures. Improved Oil and Gas Recovery, 1.

Manrique, E.J., Muci, V.E., Gurfinkel, M.E., 2007. EOR field experiences in carbonate reservoirs in the United States. SPE Reservoir Evaluation & Engineering, 10(06): 667-686.

Multiphysics, C., 2013. Comsol multiphysics reference manual. COMSOL: Grenoble, France: 1084.

Neshat, S.S., Pope, G.A., 2017. Compositional Three-Phase Relative Permeability and Capillary Pressure Models Using Gibbs Free Energy, SPE Reservoir Simulation Conference. Society of Petroleum Engineers.

O'Neill, N., 1988. Fahud field review: a switch from water to gas injection. Journal of petroleum technology, 40(05): 609-618.

Panda, M., Ambrose, J.G., Beuhler, G., McGguire, P.L., 2009. Optimized eor design for the Eileen west end area, Greater Prudhoe bay. SPE Reservoir Evaluation & Engineering, 12(01): 25-32.

Pariani, G., McColloch, K., Warden, S., Edens, D., 1992. An approach to optimize economics in a West Texas CO2 flood. Journal of Petroleum Technology, 44(09): 984-1,025.

Parsaei, R., Chatzis, I., 2011. Experimental investigation of production characteristics of the gravity-assisted inert gas injection (GAIGI) process for recovery of waterflood residual oil: effects of wettability heterogeneity. Energy & fuels, 25(5): 2089-2099.

Pinder, G.F., Gray, W.G., 2008. Essentials of multiphase flow and transport in porous media. John Wiley & Sons.

Pizarro, J.O.D.S., Branco, C.C.M., 2012. Challenges in implementing an EOR project in the pre-salt province in Deep Offshore Brasil, SPE EOR Conference at Oil and Gas West Asia. Society of Petroleum Engineers.

Ramirez, B.A., Kazemi, H., Al-Kobaisi, M., Ozkan, E., Atan, S., 2007. A Critical Review for Proper Use of Water-Oil-Gas Transfer Functions in Dual-Porosity Naturally Fractured Reservoirs-Part I, SPE Annual Technical Conference and Exhibition. Society of Petroleum Engineers.

Ranaee, E., Porta, G.M., Riva, M., Blunt, M.J., Guadagnini, A., 2015. Prediction of three-phase oil relative permeability through a sigmoid-based model. Journal of Petroleum Science and Engineering, 126: 190-200.

Rezaei, N., Firoozabadi, A., 2014. Pressure evolution and production performance of waterflooding in n-heptane-saturated fired berea cores. SPE Journal, 19(04): 674-686.

Righi, E.F. et al., 2004. Experimental study of tertiary immiscible WAG injection, SPE/DOE Symposium on Improved Oil Recovery. Society of Petroleum Engineers.

Sabti, M., Alizadeh, A., Piri, M., 2016. Three-phase flow in fractured porous media: experimental investigation of matrix-fracture interactions, SPE Annual Technical Conference and Exhibition. Society of Petroleum Engineers.

Sahimi, M., 2011. Flow and transport in porous media and fractured rock: from classical methods to modern approaches. John Wiley & Sons.

Schmid, K., Geiger, S., 2013. Universal scaling of spontaneous imbibition for arbitrary petrophysical properties: Water-wet and mixed-wet states and Handy's conjecture. Journal of Petroleum Science and Engineering, 101: 44-61.

Shahverdi, H., Sohrabi, M., 2012. Three-phase relative permeability and hystresis model for simulation of water alternating gas (WAG) injection, SPE Improved Oil Recovery Symposium. Society of Petroleum Engineers.

Shahverdi, H., Sohrabi, M., 2013. An improved three-phase relative permeability and hysteresis model for the simulation of a water-alternating-gas injection. Spe Journal, 18(05): 841-850.

Shedid, S.A., 2006. Influences of fracture orientation on oil recovery by water and polymer flooding processes: An experimental approach. Journal of Petroleum Science and engineering, 50(3-4): 285-292.

Skjaeveland, S., Siqveland, L., Kjosavik, A., Hammervold, W., Virnovsky, G., 1998. Capillary pressure correlation for mixed-wet reservoirs, SPE India Oil and Gas Conference and Exhibition. Society of Petroleum Engineers.

Stone, H., 1970. Probability model for estimating three-phase relative permeability. Journal of Petroleum Technology, 22(02): 214-218.

Stone, H., 1973. Estimation of three-phase relative permeability and residual oil data. Journal of Canadian Petroleum Technology, 12(04).

Van Dijke, M.I.J., Sorbie, K.S., 2003. Pore-scale modelling of three-phase flow in mixed-wet porous media: multiple displacement chains. Journal of Petroleum Science and Engineering, 39(3-4): 201-216.

Van Dijkum, C., Walker, T., 1991. Fractured Reservoir Simulation and Field Development, Natih Field, Oman, SPE Annual Technical Conference and Exhibition. Society of Petroleum Engineers.

Virnovsky, G., Vatne, K., Iversen, J., Signy, C., 2004. Three-phase capillary pressure measurements in centrifuge at reservoir conditions, Proceedings SCA2004-19, paper for the International Symposium of the Society of Core Analysts, Abu Dhabi.

Zendehboudi, S., Rezaei, N., Chatzis, I., 2012. Effects of fracture properties on the behavior of free-fall and controlled gravity drainage processes. Journal of Porous Media, 15(4).

Zendehboudi, S., Chatzis, I., Shafiei, A., Dusseault, MB., 2011a. Empirical modeling of gravity drainage in fractured porous media. Energy & Fuels, 25 (3): 1229-1241.

Zendehboudi, S., Chatzis, I., Mohsenipour, AA., Elkamel, A., 2011b. Dimensional analysis and scale-up of immiscible two-phase flow displacement in fractured porous media under controlled gravity drainage. Energy & Fuels, 25 (4), 1731-1750.

Zendehboudi, S., Rezaei, N., Chatzis, I., 2011c. Effect of wettability in free-fall and controlled gravity drainage in fractionally wet porous media with fractures. Energy & Fuels, 25 (10): 4452-4468.

Zhou, Y., Helland, J.O., Hatzignatiou, D.G., 2016. Computation of three-phase capillary pressure curves and fluid configurations at mixed-wet conditions in 2D rock images. SPE Journal, 21(01): 152-169.